Chapter for "Meteorites and the Early Solar System II"
D. Lauretta, L. A. Leshin, and H. Y. McSween Jr., eds.

Origin and Evolution of Carbonaceous Presolar Grains in Stellar Environments

Thomas J. Bernatowicz
Department of Physics, Washington University, Campus Box 1105, One Brookings Drive, St Louis, MO 63130-4899;
tom@wustl.edu

Thomas K. Croat
Department of Physics, Washington University, Campus Box 1105, One Brookings Drive, St Louis, MO 63130-4899;
tkc@wuphys.wustl.edu

Tyrone L. Daulton
Marine Geosciences Division, Naval Research Laboratory, Stennis Space Center, MS 39529-5004;
tdaulton@nrlscc.navy.mil

ABSTRACT

Laboratory microanalyses of presolar grains provide direct information on the physical and chemical properties of solid condensates that form in the mass outflows from stars. This information can be used, in conjunction with kinetic models and equilibrium thermodynamics, to draw inferences about condensation sequences, formation intervals, pressures and temperatures in circumstellar envelopes and in supernova ejecta. We review the results of detailed microanalytical studies of the presolar graphite, presolar silicon carbide and the nanodiamonds found in primitive meteorites. We illustrate how these investigations, together with astronomical observation and theoretical models, provide detailed information on grain formation and growth that could not be obtained by astronomical observation alone.

1. INTRODUCTION

In recent years the laboratory study of presolar grains has emerged as a rich source of astronomical information about stardust, as well as about the physical and chemical conditions of dust formation in circumstellar mass outflows and in supernova (SN) ejecta. Presolar grains isolated from primitive meteorites are studied by a variety of microanalytical techniques, leading to a detailed knowledge of their isotopic and chemical compositions, as well as their physical properties. The isotopic compositions of individual grains, obtained by ion microprobe analyses and interpreted with the aid of nucleosynthesis models and astrophysical data, help to identify the specific types of stellar sources in whose mass outflows the grains condensed. They also yield insights into stellar nucleosynthesis at an unprecedented level of detail (see Bernatowicz and Walker, 1997; Bernatowicz and Zinner, 1997; Zinner, 1998; Nittler, 2003; Clayton and Nittler, 2004; Meyer and Zinner, 2005). Mineralogical, microchemical and microstructural studies by scanning electron microscopy (SEM) and by transmission electron microscopy (TEM) of presolar grains provide unambiguous information about the kinds of astrophysical solids that actually form. With the help of kinetic and thermochemical models, SEM and TEM observations may also be used to infer the conditions of grain condensation in circumstellar dust shells. In addition, because the grains must have traversed the interstellar medium (ISM) prior to

their incorporation into the solar nebula, they serve as monitors of physical and chemical processing of grains in the ISM (Bernatowicz *et al*., 2003).

In this review we focus on carbonaceous presolar grains. Even though presolar silicates (Messenger *et al*., 2003; Nguyen and Zinner, 2004; Mostefaoui and Hoppe, 2004; Nagashima *et al*., 2004) and oxide grains such as spinel, corundum and hibonite (see Meyer and Zinner, 2005 and references therein) are important and abundant presolar minerals, few detailed laboratory data have been obtained thus far on their mineralogy and structure. An exception is the correlated TEM–ion microprobe study of presolar corundum grains by Stroud *et al.* (2004).

The situation is different for presolar silicon carbide (SiC) and graphite. Detailed structural and chemical microanalytical studies have been performed on circumstellar SiC (Daulton *et al*., 2002; 2003) and graphite (Bernatowicz *et al*., 1996; Croat *et al*., 2005b) from asymptotic giant branch (AGB) stars, and on graphite formed in SN outflows (Croat *et al*., 2003). In the present work we illustrate how microanalytical data on presolar SiC and graphite grains, interpreted with the aid of kinetic and equilibrium thermodynamics models, can be combined with astronomical observations to yield new insights into the grain formation conditions in circumstellar envelopes and SN ejecta. We also discuss the results of microanalytical studies of nanodiamonds from meteorites and interplanetary dust particles (IDPs), some components of which probably originate in supernovae.

2. AGB CARBON STARS: ASTRONOMICAL CONTEXT OF PRESOLAR GRAPHITE AND SILICON CARBIDE

Isotopic studies of presolar SiC grains from meteorites indicate that the vast majority of them originate in the mass outflows of low- to intermediate-mass carbon AGB stars, as discussed by Meyer and Zinner (2005). A small fraction (~1%) of SiC grains originate in SN ejecta, but lacking TEM data on such grains, we will set them aside in the present review. For presolar graphite the distribution of grains among astronomical sources is less clear. Low density graphite spherules from the KE3 separate of the Murchison meteorite (1.65 – 1.72 g/cm^3; Amari *et al*., 1994) tend to be large (mean diameter ~6 μm) and generally show evidence of SN origin. High-density graphite spherules from the KFC1 separate (2.15 – 2.20 g/cm^3; Amari et al., 1994) are more numerous but are typically smaller (mean diameter ~ 2 μm; cf. Bernatowicz *et al*., 1996), and seem to originate predominately in carbon AGB stars (Croat *et al*., 2005a; 2005b). The specification of *carbon* AGB stars comes from the simple thermochemical consideration that in order for these carbonaceous grains to form it is required that C/O > 1 in the gas phase, because at lower values all C is tied up in the very stable CO molecule. It is only when the C number density exceeds that of O that sufficient carbon is available to form graphite and carbides (Lodders and Fegley, 1995; Sharp and Wasserburg, 1995). SiC is indeed observed astronomically around carbon stars (e.g., Speck *et al*., 1999), supporting the identification of carbon stars as a source of presolar SiC.

In the present work we do not give a treatment of stellar evolution and nucleosynthesis, so the reader may wish to consult the review by Lattanzio and Boothroyd (1997) on the evolution of stars from the main sequence to the mass-losing Asymptotic Giant Branch (AGB) phase. We also do not treat the rather complex nomenclature of carbon stars. Instead, we refer the reader to the discussion of their classification and properties presented by Lodders and Fegley (1997).

The physical characteristics of present day carbon stars are represented in Figure 1, a small portion of the Hertzsprung-Russell (HR) diagram that we have adapted from Figure 9 of Bergeat

et al. (2002a), depicting a large number (~300) of carbon stars studied by HIPPARCHOS (ESA, 1997). Loci of constant stellar radius (in multiples of the solar radius $R_\odot$) are indicated as diagonal lines. For reference, the Sun resides on the main sequence (off the diagram at lower left), at an effective temperature of 5770 K and bolometric magnitude M_{bol} = +4.75 (Log $L/L_\odot$= 0). The carbon stars in Figure 1 are broadly classified as HC ("hot carbon") stars, CV ("carbon variable") stars, and Tc ("technetium") stars. The HC group consists largely of stars that have non-variable light, but also includes some irregular and small-amplitude variables, carbon cepheids, and RCrB variables. The R-stars are mostly included in this group. CV stars are cool, long period variable stars (Miras) whose luminosities, effective temperatures and radii vary periodically with time. They include the N-stars and the late stage R-stars that can be explained by the third dredge-up, and are close to the tip of the thermally pulsing AGB region of the HR diagram. The Tc stars are CV giants that have detectable technetium in their atmospheres, indicating a recent dredge-up of s-process material. The general trends for CV stars are that with increasing stellar luminosity and decreasing effective temperature, the stellar masses, C/O ratios and atmospheric opacities increase.

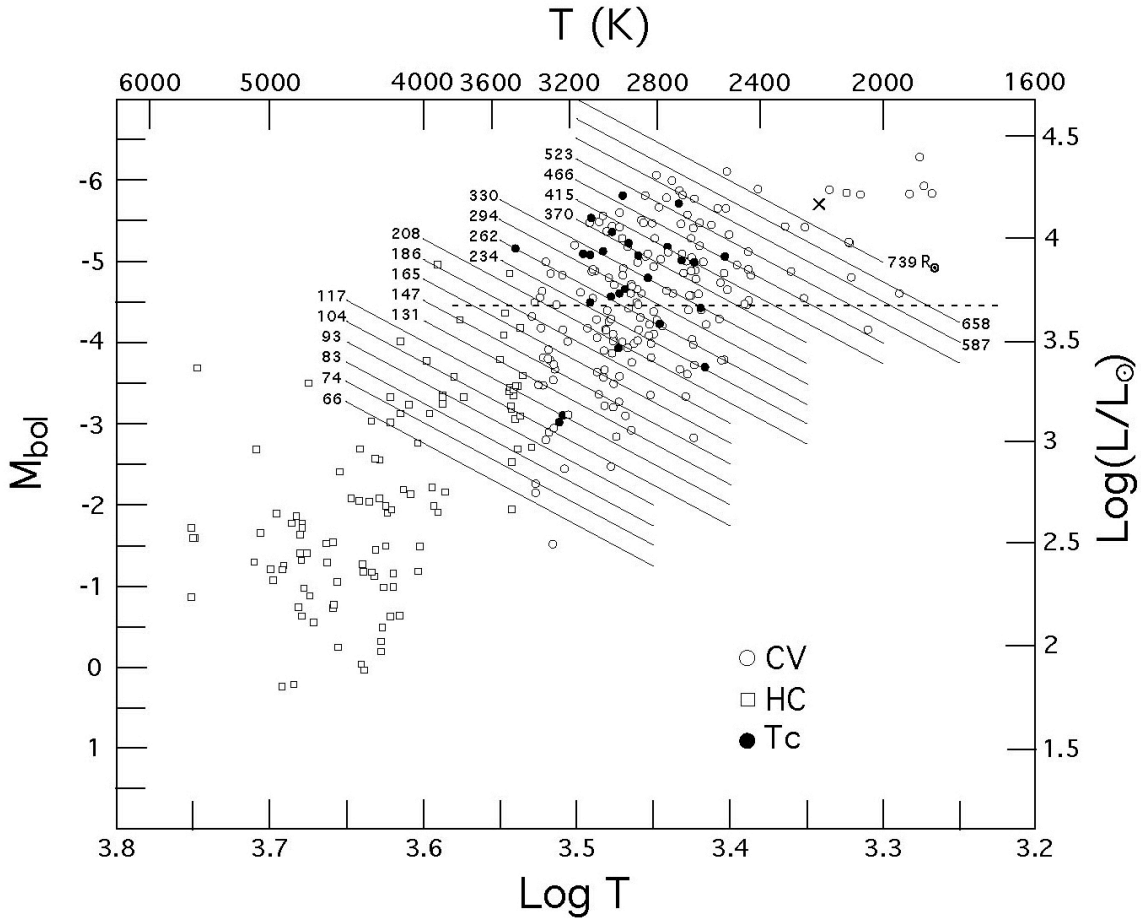

Figure 1. Bolometric magnitude (M_{bol}) vs. effective temperature (T) for ~ 300 carbon stars (HR diagram), adapted from Bergeat *et al*. (2002a). CV = variable carbon giants, HC = hot carbon stars, Tc = variable carbon giants with detectable technetium. Loci of constant stellar radius (in terms of the solar radius $R_\odot$) are indicated. The dashed horizontal line at 4700 $L_\odot$ corresponds to carbon stars with M = 1.1 $M_\odot$, the minimum mass needed for a star to have evolved sufficiently rapidly to have contributed grains to the solar nebula. The closest and best studied variable carbon star IRC +10216 is shown as the x-symbol.

Not all of the types of carbon stars shown in Figure 1 are possible contributors of dust to the solar nebula, as discussed by Bernatowicz *et al*. (2005). In this regard, the most fundamental distinction that can be made is on the basis of stellar mass, because it is only stars that have sufficient mass that would have evolved rapidly enough on the main sequence to have contributed dust to the solar nebula. The lifetime t_* of a star on the main sequence varies in proportion to its mass M_*, and varies inversely as the power radiated by the star (its luminosity L_*). The luminosity is, in turn, proportional to M_*^K, where K = 3.5 classically. Data from HIPPARCOS, however, suggest that the exponent is better determined as K = 3.7 for $M_* \shortparallel 0.5 - 5\ M_\odot$ (Lampens *et al.,* 1997; Martin *et al*., 1998). The stellar main sequence lifetime t_* is then given in terms of the solar main sequence lifetime $t_\odot$ as

$$t_* = t_\odot\,(M_*/M_\odot)^{-2.7} \qquad (1)$$

with $t_\odot \shortparallel 10$ - 11 Gy (Iben, 1967; Sackmann *et al*., 1993). Since significant mass loss occurs only at the end of their lifetimes, pre-solar stars must have evolved beyond the main sequence to have contributed dust to the solar nebula. The maximum lifetime t_* of stars (and therefore their minimum mass) that contributed matter to the Solar System is then constrained to be approximately the difference between the age of the Galaxy t_{Galaxy} and the age t_{SS} of the Solar System, that is, $t_* \lesssim t_{Galaxy} - t_{SS}$. The latter quantity is well determined as t_{SS} = 4.6 Gy, while the former quantity may be estimated from the recent WMAP age of the Universe (13.7 ± 0.2 Gy; Bennett *et al.* 2003). Using these numbers we would find $t_* \lesssim 9.1$ Gy (and from Eq. [1], $M_* \gtrsim 1.04\ M_\odot$).

This t_* is, however, really an extreme upper limit on the lifetime of stars that could have contributed dust to the solar mixture for two reasons. First, t_{Galaxy} is estimated to be less than the age of the Universe by ~1 Gy, based on recent constraints on the age of globular clusters (Krauss and Chaboyer, 2003). Second, the limit on t_* implicitly includes the residence lifetime in the ISM of the matter expelled from stars prior to its incorporation in the solar nebula. There are currently no reliable data on the ISM residence lifetimes of presolar grains, but an estimate may be made using theoretical lifetimes of ≲0.5 Gy against grain destruction in the ISM (see Jones *et al.* 1997). With these considerations, we estimate $t_* \lesssim 7.5$ - 8 Gy. As equation (1) shows, M_* is relatively insensitive to the uncertainty in the stellar lifetime, varying approximately as the inverse cube root of t_*. For t_* in the estimated range, we find $M_* \gtrsim 1.1\ M_\odot$. We therefore take this as the minimum mass for stars *of any kind* that could have contributed grains to the solar nebula.

It is important to note here that the mass range in which *carbon* stars are capable of forming is more restricted on theoretical grounds, both at low and high mass limits. Gallino *et al*. (1997) argue that below ~1.3 $M_\odot$, mass loss may cause such stars to undergo too few of the third dredge-up events necessary to evolve into carbon stars, prior to their evolving into white dwarfs. On the other hand, stars with masses much greater than ~4 - 5 $M_\odot$ may be subject to hot-bottom burning, which also drastically limits carbon and s-process element enrichment. These limits are subject to uncertainties that are difficult to evaluate, but are broadly consistent with observation.

The mass-luminosity relation for AGB carbon stars derived by Bergeat *et al*. (2002b), for which the stellar luminosity varies approximately as the square root of the stellar mass, implies a minimum luminosity $L_* \gtrsim 4700\ L_\odot$ (M_{bol} = - 4.46) for carbon stars of $M_* \gtrsim 1.1\ M_\odot$ that could have contributed SiC and graphite grains to the solar nebula (Bernatowicz *et al*., 2005). This luminosity threshold is shown as a dashed horizontal line in Figure 1. It can be seen that this

threshold excludes all but two of the HC stars, effectively eliminating stars of this group as potential contributors of presolar grains. Consequently, it is the long period variable carbon (CV) stars of mass $M_* \gtrsim 1.1\ M_\odot$ that are implicated as the probable sources of meteoritic presolar graphite and SiC grains that carry enhancements of s-process elements.

The lower limit on the luminosity of carbon stars that were capable of contributing grains to the solar nebula constrains their range of effective temperatures from $T \sim 1900$ K – 3400 K, their luminosities from $L \sim 4700\ L_\odot - 19{,}500\ L_\odot$, and their radii from $R \sim 200\ R_\odot - 1300\ R_\odot$ (Fig. 1). A comparatively small number of stars, namely very cool, highly luminous ones (including the nearest and well-studied carbon star IRC +10216), populate one extreme edge of this range. All of the stars above the luminosity threshold of 4700 $L_\odot$ (for $M_* \gtrsim 1.1\ M_\odot$) are giants, as can be appreciated from noting that even the smallest have radii of about 1 A.U. (215 $R_\odot$). The most densely populated portions of this region of the HR diagram correspond to stars with temperatures from $T = 2240$ K – 3350 K and luminosities from $L = 4700\ L_\odot - 15{,}500\ L_\odot$. This luminosity range translates into masses from $M = 1.1 - 8\ M_\odot$, using the mass-luminosity relation for CV stars. The CV stars in this range of temperature and luminosity have mean fundamental pulsation periods of about 1 ± 0.4 y (Bergeat *et al*., 2002b).

To relate the origin of presolar SiC and graphite more securely to carbon AGB stars, it is also necessary to consider the isotopic compositions of the grains. Nucleosynthesis models suggest that low-mass (~1 – 3 $M_\odot$) AGB carbon stars are responsible for the majority (> 95%) of presolar SiC grains (see Daulton *et al*., 2003 and references therein). The $^{12}C/^{13}C$ distribution for presolar SiC lies mainly within $^{12}C/^{13}C = 30$ - 100, with a maximum in the distribution at 50 - 60 (Hoppe and Ott 1997; cf. solar $^{12}C/^{13}C = 89$), similar to the distribution for N-type carbon star atmospheres (Lambert *et al*., 1986). The similarity of these isotopic distributions is compelling evidence for the AGB origin of most presolar SiC. A small fraction of SiC (~5%) grains have $^{12}C/^{13}C$ ratios < 10 and possibly originate from J-type carbon stars. An even smaller fraction (~1%) originates in SN outflows, based mainly on observed excesses of ^{28}Si (which can only be produced in the deep interiors of massive stars: see Zinner, 1998; Nittler, 2003; Meyer and Zinner, 2005). The majority of these SiCs of SN origin have $^{12}C/^{13}C > 100$, up to ratios of several thousand.

The $^{12}C/^{13}C$ ratios of presolar graphites from AGB stars span a much larger range than those of SiCs from AGB stars. In the Murchison meteorite KFC1 high-density graphite separate (mean diameter ~ 2 μm; 2.15-2.20 g/cm^3; Amari *et al*., 1994) about 10% of the graphites have $^{12}C/^{13}C < 20$, but about 2/3 of them have isotopically light carbon ($100 \lesssim {}^{12}C/^{13}C \lesssim 5000$; cf. Bernatowicz *et al*., 1996). Noble gas isotopic compositions of these graphites suggest an AGB origin (Amari *et al*., 1995b). However, there is a prominent gap in the distribution of $^{12}C/^{13}C$ ratios for graphite that corresponds roughly to the peak in the distribution of AGB SiC. This suggests that graphite may be produced at a different stage in the evolution of low mass carbon stars, or else by carbon stars of different mass and/or metallicity than those that produce SiC. Two lines of evidence suggest the latter possibility. First, AGB graphites often contain internal crystals of carbides enriched in s-process transition metal elements (e.g., Zr, Mo, and Ru; Bernatowicz *et al*., 1996; Croat *et al*., 2004; 2005a; 2005b). This is a clear indication of formation around late stage AGB stars, where third dredge-up events transport ^{12}C from 3α He-burning as well as s-process elements to the stellar surface. Nucleosynthesis models (Amari *et al*., 2001) suggest that low metallicity AGB stars can produce the observed light carbon as well as the s-process enrichments in Zr, Mo, and Ru needed to condense carbides of these elements. Second, NanoSIMS determinations of Ti isotopic compositions in TiC within KFC1 graphites

(Amari *et al.,* 2004) often show excesses in ^{46}Ti and ^{49}Ti relative to ^{48}Ti (with ^{49}Ti/^{48}Ti as high as 5 times the solar ratio), consistent with neutron capture in the He intershell during the third dredge-up in thermally pulsing AGB stars. The light carbon isotopic compositions of most KFC1 graphites, as well as their Ti isotopic compositions, are consistent with an origin around intermediate-mass carbon stars with $M \gtrsim 3\ M_{\odot}$.

3. SILICON CARBIDE FROM CARBON STARS

SiC was first observed in the dusty envelopes of carbon stars from a relatively broad 11.3 μm infrared (IR) feature attributed to emission between the transverse and longitudinal optical phonon frequencies (Treffers and Cohen, 1974; Forrest *et al.*, 1975). On the basis of laboratory studies of SiC synthesis, it is expected that the physical characteristics of SiC formed around carbon stars, such as grain size and microstructure, will depend on physical conditions in the circumstellar outflows, and thus could provide information on these conditions. Astronomical data are of limited use in this regard. For example, SiC is known to form on the order of a hundred different polytypes in the laboratory (the unique cubic 3C polytype, also called β-SiC, and hexagonal and rhombohedral polytypes, collectively termed α-SiC; Figure 2). However, astronomical data have only been shown capable of distinguishing between the 3C and 6H polytypes, and even whether this distinction can be made on the basis of astronomical IR-spectra has been the subject of controversy (see Speck *et al.,* 1997; 1999). On the other hand, if the presolar SiC extracted from meteorites can be taken to represent a fair sample of the types of SiC produced by various stellar sources (with $\gtrsim$ 95% from carbon stars), then laboratory studies of these grains provide direct information about the microstructure of the grains formed in these astronomical environments, and can help to infer the physical conditions of their formation.

With this idea in mind, Daulton *et al*. (2002; 2003) determined the polytype distribution of astronomical SiC by analytical and high-resolution transmission electron microscopy (HR-TEM) of many hundreds of presolar SiC grains from the Murchison CM2 carbonaceous meteorite. They demonstrated that, aside from a small (1% by number) population of one-dimensionally disordered SiC grains, only two polytypes are present -- the cubic 3C (β-SiC) polytype (~79%) and the hexagonal 2H (α-SiC) polytype (~3%) as well as intergrowths (Figure 3) of these two polytypes (17%). It is interesting to note that, prior to the Daulton *et al*. (2002) study of SiC from Murchison, 2H SiC had never been observed to occur in nature.

Broadly speaking, studies of SiC synthesis show that the 2H polytype has the lowest formation temperature. As temperature is increased, the next SiC polytype to form is 3C. If temperature is increased further, 2H SiC formation ceases. Cubic 3C SiC has a wide range of growth temperatures and the general trend is that higher order SiC polytypes begin to grow along with 3C SiC, until temperatures exceed the 3C formation range. Thus, 2H and 3C can be considered the lowest temperature SiC polytypes. Temperatures at which 2H SiC are known to grow and remain stable (~ 1470 - 1720 K; see Daulton *et al.,* 2003 and references therein) largely fall within the temperature range predicted by equilibrium thermodynamics for SiC formation in circumstellar outflows (see Section 4).

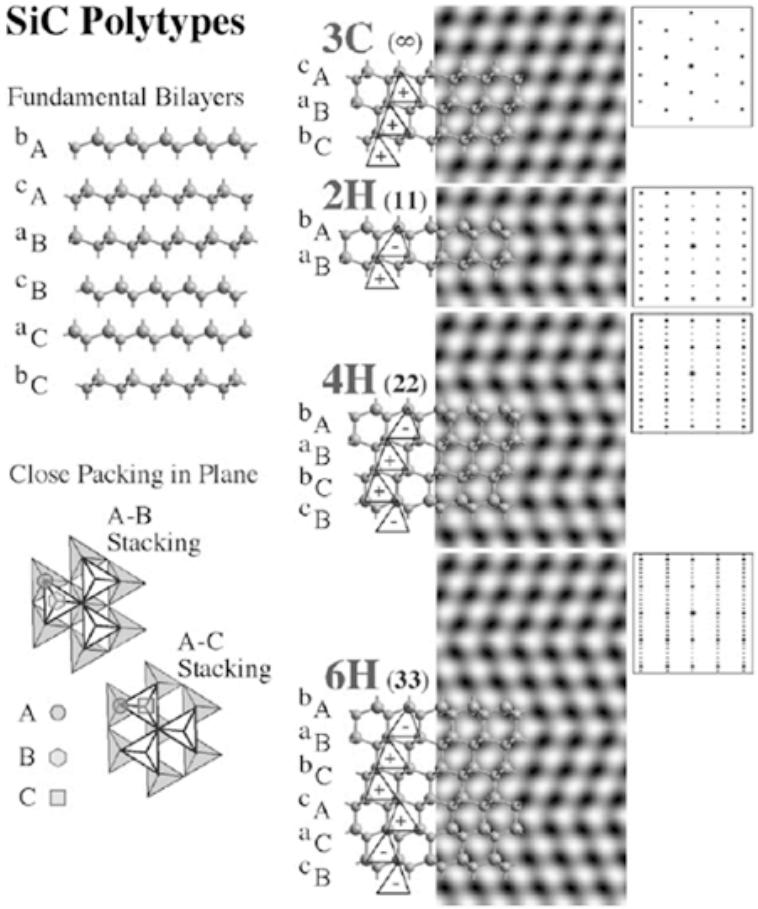

Figure 2. Silicon carbide polytype structures. Polytypes of SiC are formed by those periodic stacking sequences of bilayers that produce tetrahedral sheets. Atomic models of the six unique (fundamental) bilayers (*bA*, *cA*, *aB*, *cB*, *aC*, and *bC)* of SiC (top left) based on three principle close packed planes (*A*, *B*, and *C*) (lower left) are shown. Smaller atoms represent C and larger atoms represent Si. The two basic stacking arrangements, *A-B* and *A-C*, that form planes of vertex-sharing parallel and antiparallel tetrahedra, respectively, are shown (lower left). Atomic models of the four simplest (3C, 2H, 4H, and 6H) polytypes are shown superimposed on calculated high resolution TEM lattice images produced using defocus conditions that reproduce the symmetry of the projected lattice (center column). Schematic illustrations of electron diffraction patterns (including forbidden reflections in some cases) are also shown (right column). From Daulton *et al*. (2003).

Because pressures in these outflows are low, SiC condensation cannot take place until temperatures drop well below 2000 K, less than the experimental formation temperatures of most SiC polytypes. Indeed, comparison of the equilibrium thermodynamics condensation temperatures with experimental data on the formation of SiC polytypes leads to the conclusion that *only* 2H and 3C polytypes are likely to form in circumstellar atmospheres, in agreement with observation.

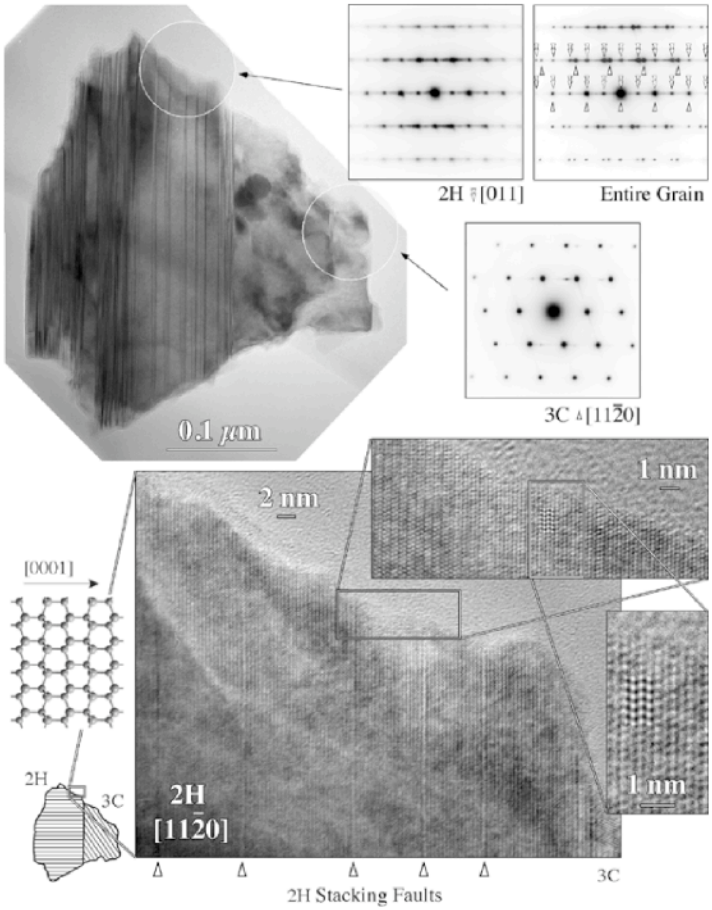

Figure 3. TEM study of a presolar SiC grain from the Murchison meteorite, an intergrowth of 2H and 3C polytypes. The selected area electron diffraction pattern for the entire grain is a composite of diffraction patterns from the 2H [$11\bar{2}0$] and 3C [011] oriented SiC domains. A bright field image of the grain is shown along with progressively magnified high-resolution lattice images showing cross-lattice planes. Inset in the high-resolution image is a simulated lattice image calculated under defocus/thickness conditions which match the lattice fringes in the micrograph. Long-range 2H order is evident in the lattice images of the 2H SiC domain. From Daulton *et al.* (2003).

Daulton *et al.* (2002; 2003) proposed a simple hypothesis to account for the observed polytypes and their relative abundances, namely that 3C SiC first condensed at small radii (higher temperatures) and 2H SiC condensed later at larger radii (lower temperatures) in AGB atmospheres. At intermediate radii in the SiC growth region, intergrowth grains might form directly or by 2H heteroepitaxial growth on preexisting 3C SiC grains that were transported to cooler regions in AGB mass outflows by stellar radiation pressure. The observed relative abundances 3C and 2H SiC are consistent with this hypothesis. Since the rate of grain nucleation from the gas varies as the square of the number density of gas species contributing to grain growth (McDonald, 1963), polytypes nucleating at higher temperatures and higher gas number densities should be more abundant than polytypes nucleating later at lower temperatures and lower number densities in the expanding outflow. The nucleation rate of lower temperature forms of SiC should also be reduced because of the prior removal of Si into the SiC already formed at higher temperatures. In accord with these expectations, single crystals of 3C SiC,

which formed at higher temperatures than 2H SiC and therefore at higher gas phase Si number densities, are far more numerous than single crystals of 2H SiC.

Reliable constraints on the conditions in AGB star outflows also come from the application of equilibrium thermodynamics to the chemical composition of presolar grains (see Section 4). For example, Lodders and Fegley (1997) noted that the pattern of trace element enrichment seen in "mainstream" presolar SiC is exactly mirrored in the elemental depletion patterns observed astronomically in the atmospheres of N-type carbon stars. They showed that these depletion patterns are consistent with the trace element partitioning into condensing SiC predicted by equilibrium thermodynamics.

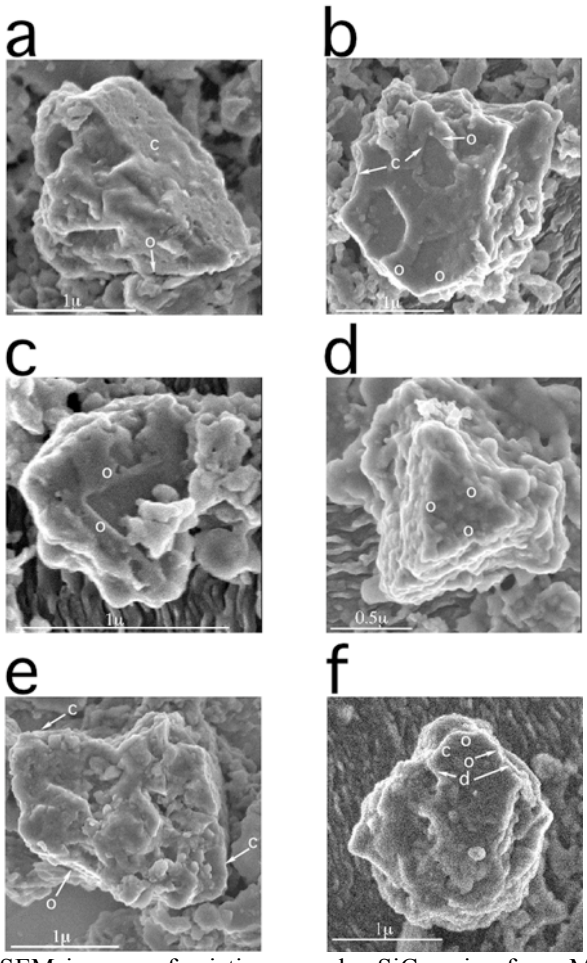

Figure 4. Field emission SEM images of pristine presolar SiC grains from Murchison exhibiting primary growth crystal faces (a-f) and polygonal depressions (a-c). Scale bars are 1 μm, except for (d) where the scale bar is 0.5 μm. Letter labels within panels indicate forms for cubic crystals: c = cube, o = octahedron; and d = dodecahedron. Panels (a) - (d) show "euhedral" crystals with well-developed faces. Panels (e) and (f) show subhedral crystals with few and/or imperfectly developed faces. From Bernatowicz *et al*., 2003.

Information obtained by studying the external morphology of presolar SiC grains complements that gained by studying its internal structure. Bernatowicz *et al*. (2003) developed a technique involving gentle disaggregation of primitive meteorites, X-ray mapping by SEM, followed by high resolution imaging in the field emission SEM, to locate presolar SiC grains and study their surfaces. These "pristine" SiC grain surfaces are in a state that reflects their natural history--their formation, journey through the ISM, incorporation into the solar nebula and

meteorite parent body-- rather than laboratory artifacts induced by the chemical etching that is generally used to isolate SiC for isotopic studies.

About 90% of pristine SiC grains are bounded by one or more crystal faces. Polygonal depressions (generally < 100 nm deep) are observed in more than half of these crystal faces, and commonly have symmetries consistent with the structure of the 3C polytype (Figures 4a-c). Comparison of these features with the surface features present on heavily etched presolar SiC grains from Murchison separate KJG (Amari *et al.*, 1994), indicate that the polygonal depressions on pristine grains are primary features, resulting from incomplete convergence of surface growth fronts during grain formation. The chemically etched presolar SiCs have high densities of surface pits (probably etched linear defects) in addition to the polygonal depressions seen on pristine grains. The inferred defect densities are quite high (as much as $10^8 - 10^9$ /cm^2), about $10^3 - 10^4$ times higher than in synthetic SiCs that are engineered to minimize defects. Taken together, the polygonal depressions and the high defect densities indicate rapid initial growth of presolar SiC that was kinetically quenched when the gas phase became too rarefied.

In their study of pristine SiC, Bernatowicz *et al.* (2003) confirmed an observation of Alexander *et al.* (1990), based on *in situ* characterization of SiC in meteorite matrices, that no other primary condensates are intergrown with or overgrown on presolar SiC. The absence of other primary condensates indicates that further growth or back-reaction with the gas phase became kinetically inhibited as the gas densities in the expanding AGB stellar atmospheres became too low. This has the important implication that primary oxide or silicate minerals sheathing SiC grains cannot have been responsible for their survival in the solar nebula. SiC volatilization experiments by Mendybaev *et al.* (2002) have shown that the lifetimes of presolar SiC grains exposed to a hot ($T \geq 900^oC$) solar nebula are quite short (< several thousand years) compared to nebular cooling timescales. The survival of the SiC grains that are found in meteorites, as well as the often exquisite state of preservation of their surfaces, thus implies that some SiC entered the solar nebula late and/or in its outer, cooler parts. However, there is evidence that some of the surviving presolar SiCs were surficially oxidized. Stroud and Bernatowicz (2005) studied a focused ion beam section of a pristine SiC grain by TEM that had a 10 – 30 nm rim of silicon oxide.

4. GRAPHITE FROM CARBON STARS

As noted in Section 2, the isotopic compositions of graphites from the KFC1 separate of the Murchison meteorite (Amari *et al*., 1994) indicate an origin in AGB stars for most of them. Ultramicrotome sections of many hundreds of these graphites have been the subject of detailed TEM studies (Bernatowicz *et al*., 1996; Croat *et al.,* 2004; 2005a; 2005b). Two basic spherule types are present. These are designated “onion-type” and “cauliflower-type” based on their external morphologies in SEM images. TEM images of ultramicrotome slices of the graphite spherules show that structural differences, in the regularity of the stacking and in the long-range continuity of graphene sheets, lead to their two distinct external morphologies (Figure 5).

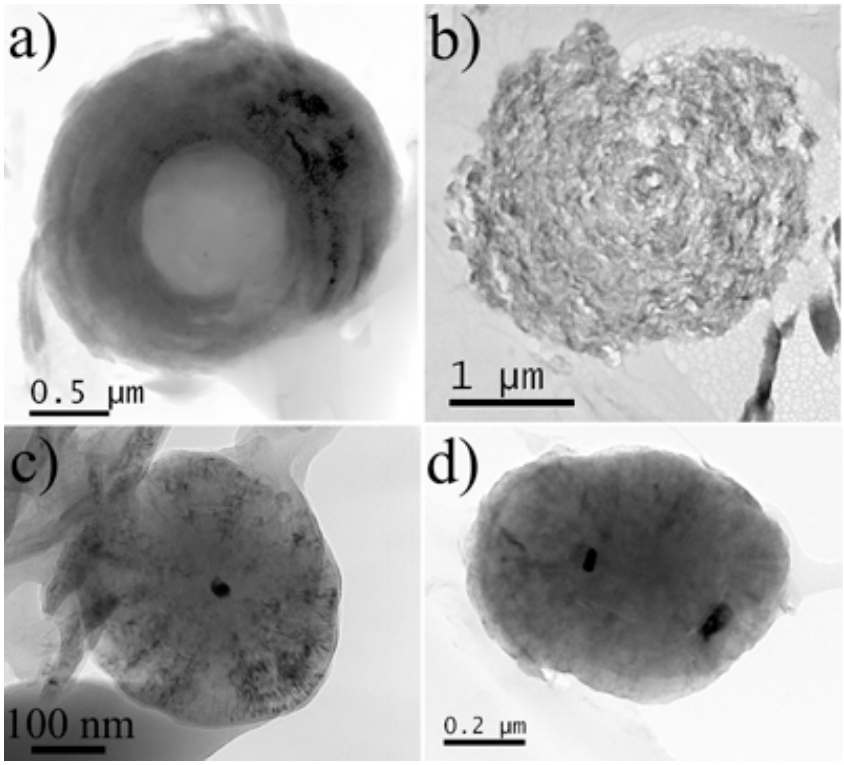

Figure 5. TEM bright-field images of 70 nm thick ultramicrotome sections of presolar graphite grains from Murchison graphite separate KFC1 (Amari *et al*., 1994): (a) Onion-type graphite with a nanocrystalline carbon core; (b) Cauliflower-type graphite; (c) Onion-type graphite with 26 nm central carbide crystal (metal composition $Ti_{80}V_7Fe_6Mo_3Zr_3Ru_1$); (d) Onion-type graphite with Zr-Mo-Ti non-central carbides (70 nm and 30 nm). These carbides have metal compositions $Zr_{83}Mo_{13}Ti_2Fe_2$ and $Zr_{86}Mo_{13}Ti_1$, respectively.

The exteriors of onion graphites are well-crystallized graphitic layers, which form concentric shells. Selected area electron diffraction (SAED) patterns from the onion layers (Figure 6) show strong (002) rings formed by planes of atoms viewed edge-on (with their c-axes perpendicular to the electron beam). Low magnification dark-field images show that the graphene planes are coarsely aligned over hundreds of nanometers, gradually curving to form the concentric layers of the onion. About two-thirds of the onion-type graphites have cores of nanocrystalline carbon (Figures 5a and 6a), consisting of small, randomly-oriented graphene sheets with a mean diameter of ~3 - 4 nm. There is no evidence of (002) layer stacking, as in normal graphite, indicating that the graphene sheets in the cores are probably curled due to insertion of pentagonal configurations of C atoms into the overall hexagonal structure of the sheets (Fraundorf and Wackenhut, 2002). The shape of diffraction peak intensity profiles also indicates that as much as one-quarter of the mass of the cores may be in form of polycyclic aromatic hydrocarbons (PAHs) or related structures (Bernatowicz *et al*., 1996). Indeed, the presence of PAHs in the onion-type graphites has been confirmed directly by two-step laser desorption-laser ionization mass spectrometry (Messenger *et al*., 1998).

Considering various possibilities for the formation of the onion-type graphites with nanocrystalline carbon cores, Bernatowicz *et al.* (1996) speculated that they formed in environments where few refractory minerals (see below) were available to serve as sites for heterogeneous nucleation, so that C condensation was delayed until homogeneous nucleation

could occur at high supersaturation levels. In this scenario, the ensuing rapid condensation resulted in the formation of isolated aromatic networks (PAHs and graphene sheets) that coalesced to form the nanocrystalline cores, which subsequently were overgrown by graphite at reduced C partial pressures. Rare aggregates of onion-type graphites are also observed. These are composite objects that apparently were created when graphites that originally formed and grew separately became attached and were cemented together during subsequent carbon condensation.

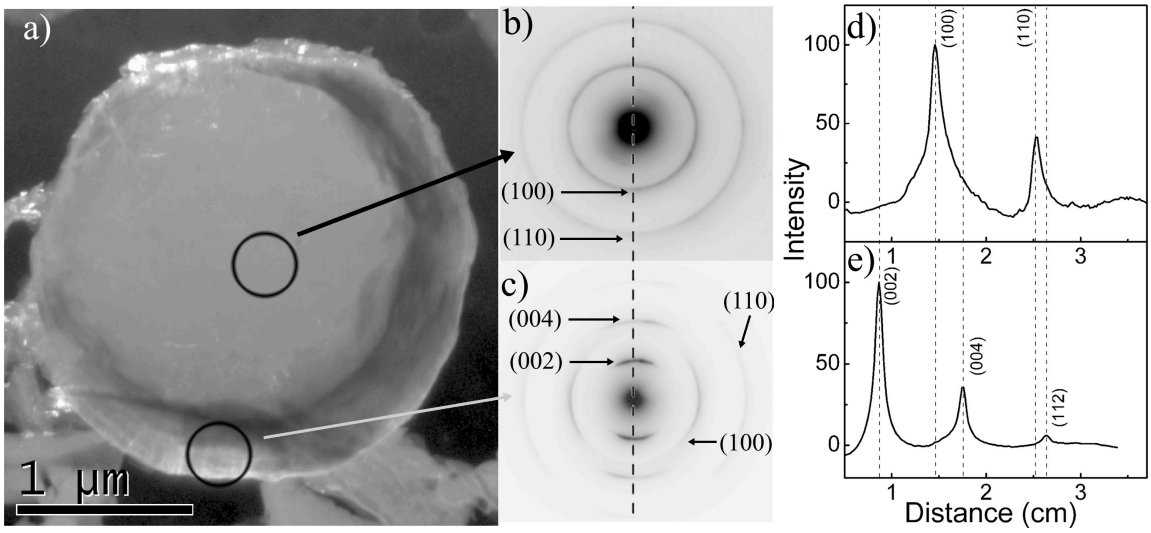

Figure 6. Dark-field (a) image of an ultramicrotome (~70 nm thick) section of a rim-core onion-type graphite from Murchison separate KFC1 (Amari *et al*., 1994). Panels (b) and (c) are selected area electron diffraction (SAED) patterns from separate ~300 nm regions of the section (with positions indicated by arrows). Note the powder-like diffraction pattern and absence of (002) and other stacking layer reflections from the core region. Line profiles of the diffracted intensity (d and e) were taken from digitized SAED patterns (along the dotted line) and major diffraction peaks are indexed with the family of planes (hkl) from the known graphite structure.

Cauliflower-type graphites (Figure 5b) show turbostratic layering, which consists of graphene sheets that are wavy and contorted. Some do show a roughly concentric structure with layers that diffract coherently over several hundred nanometers. Unlike the onion-type layering, however, these coherently scattering domains are of limited thickness (< 50 nm). The lack of orderly stacking in the c-axis direction leads to loose-packed structures, with visible gaps in cross-section, and to an apparently lower density than for onion-type graphites. Other cauliflowers are even less ordered, being devoid of concentric layers and consisting of coherent scattering domains with a maximum diameter of 20-30 nm. Whether onion-type and cauliflower-type graphites are formed in the same astrophysical environments is not known. Despite the fact that their C isotopic compositions in KFC1 span the same range and are similarly distributed, and that both types contain internal crystals of refractory carbides often enriched in s-process elements like Mo, Zr and Ru (see below), it seems probable that their different structures reflect (unknown) differences in the conditions of their formation.

Internal crystals of refractory carbides are commonly found inside of graphite from AGB stars, in both the onion (Figures 5c, 5d) and cauliflower types (e.g., Bernatowicz *et al*., 1991). These high temperature condensates were evidently ubiquitous in the gas at the time that graphite began to form. Because only one ~70 nm ultramicrotome section of any given AGB

graphite is typically examined, it is clear that the 16% frequency of occurrence of internal carbides is a strict lower limit on the fraction of graphite spherules actually containing internal grains. In some cases the carbides are nearly pure TiC (Figure 5c). Many of the carbides, however, are solid solutions that show substantial enrichments above the solar ratios in Zr, Mo, and Ru, which are elements predominantly produced by the s-process. Carbide compositions can be dominated by these s-process elements, as in Zr- Mo-carbides with Ti present at only a few atomic percent (Figure 5d). Carbides from onion-type graphites have an average geometrical mean size of 24 nm, and range from ~7 nm to a maximum of ~90 nm (Croat *et al*., 2005b). Textural evidence as well as compositional variation among carbides within a single graphite indicate that carbides form first and are then incorporated into the developing graphite, rather than forming later by exsolution (Bernatowicz *et al.,* 1996). About 40% of carbide-containing graphites have an internal grain located at the spherule center (as in Figure 5c), a clear indication of heterogeneous nucleation of graphite on preexisting carbides.

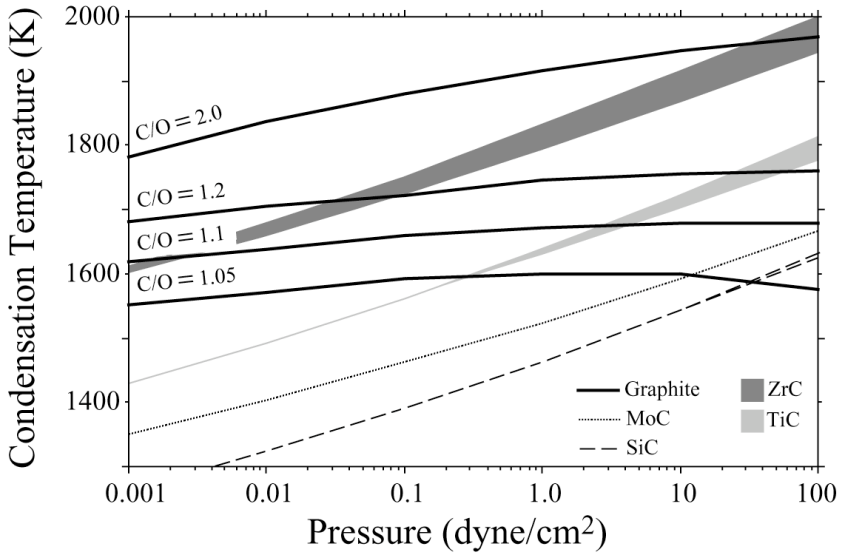

Figure 7. Equilibrium condensation temperatures for various carbides and graphite as a function of total pressure and C/O ratio (from 1.05 to 2), for solar abundances of all elements but C. Condensation temperatures for ZrC, TiC and SiC vary slightly with C/O and are displayed as envelopes. For these compounds, the lower boundary of the envelope is for C/O=1.05, and the upper boundary is for C/O ≥ 2.0. For MoC, the condensation temperature does not vary with C/O in the displayed pressure range. The condensation temperature of Mo_2C (not shown) is only a few degrees higher than for MoC at any given pressure. From Bernatowicz *et al.* (1996) using data from Lodders and Fegley (1995).

Because the AGB graphite spherules with carbides consist of at least two entirely different mineral phases, equilibrium thermodynamics may be used to constrain temperatures, pressures and gas compositions in the grain formation environment, and these predictions can be checked against astronomical observation. Figure 7 displays condensation temperatures for graphite and various carbides as a function of the gas pressure and C/O ratio, under conditions of thermodynamic equilibrium. Only ratios C/O > 1 are shown, because it is only when the C number density exceeds that of O that sufficient carbon is available to form graphite and carbides (see Lodders and Fegley, 1995; Sharp and Wasserburg, 1995). The condensation temperatures for the carbides in Figure 7 reflect solar abundances of these elements. It is clear that ZrC will

condense before TiC, and MoC after TiC, over all pressures in the range shown. With increasing degrees of s-process enrichment of Mo and Zr, however, condensation temperatures of carbides formed from these elements increase (Lodders and Fegley, 1995). For s-process elemental abundances typical of carbon star outflows (≈10-100 x solar), MoC condensation temperatures become comparable to those of TiC, and ZrC condensation temperatures increase to values ~7-10% greater than those shown.

Inspection of Figure 7 shows that the graphite condensation temperature is relatively insensitive to pressure, but strongly dependent on C/O, while carbide condensation temperatures depend on pressure but are insensitive to C/O. Since the condensation curves of the carbides cross those of graphite, whether a given carbide will start forming before or after graphite depends on the ambient pressure. The higher the C/O ratio, the greater is the pressure required for carbides to condense before graphite. It is noteworthy that the condensation temperature for SiC is well below that of graphite at even the lowest C/O ratios, for all but the highest pressures shown. This is consistent with the fact that SiC has been observed in only one KFC1 graphite out of several hundred examined.

Presolar graphites with internal crystals of TiC can be used, for example, to place firm constraints on the C/O ratios of the AGB atmospheres in which they formed. TiC will condense before graphite at $P \gtrsim 0.3$ dynes/cm^2 for C/O = 1.05, at $P \gtrsim 3$ dynes/cm^2 for C/O = 1.1, and at $P \gtrsim 30$ dynes/cm^2 for C/O = 1.2. However, the C/O ratio cannot be increased much beyond this if TiC is to condense before graphite and possibly serve as a nucleation center. As C/O approaches ~ 1.5, the required pressure reaches photospheric values for low- to intermediate-mass AGB stars (~700 – 1400 dynes/cm^2; Soker and Harpaz, 1999), but at the photosphere the temperature is far too high (~2200 K – 3400 K) for any grains to condense. Grains must instead condense in regions above the photosphere where both temperatures and pressures are much lower. The presolar graphites with nuclei of TiC thus indicate ratios of $1 \lesssim C/O \lesssim 1.2$ in the circumstellar atmospheres where they formed, as originally argued by Sharp and Wasserburg (1995).

This prediction is robust, and moreover is consistent with astronomical observations of AGB stars. Using C/O ratios for carbon stars determined by Lambert *et al*. (1986), Bergeat *et al*. (2001) calculated the mean C/O for variable carbon (CV) stars, and arrived at a mean C/O = 1.15 $\pm$ 0.16. These astronomical C/O ratios compare very favorably with the constraints on C/O derived from the interpretation of presolar graphite compositions and microstructures based on thermochemical calculations. The plausibility of the C/O ratios inferred from equilibrium thermodynamics means that reasonable confidence can be placed in the correlated physical inferences about temperatures and pressures in the circumstellar environments where the graphite and carbide grains formed.

Circumstellar grains are important not only because they provide solid matter to the ISM, but also because they play an important role in the dynamical evolution of AGB stars. The general understanding is that shocks in the stellar atmosphere above the photosphere enhance the gas density, promoting the condensation of dust. Copious mass loss from the star occurs largely because the dust is coupled to the stellar radiation field, which accelerates grains by radiation pressure. Momentum is, in turn, transferred to gas molecules by collisions with grains. The dust/gas mixture is effectively a two-component fluid whose motion and atmospheric structure are dynamically coupled: the radiation pressure on the grains determines the velocity field of the outflow and thus the density distribution, while the density distribution itself determines the conditions of radiative transfer within the outflow and thus the effective radiation pressure (see

Bowen, 1988; Netzer and Elitzur, 1993; Habing *et al.,* 1994; Ivezic *et al*., 1998; Winters *et al.,* 2000).

For the special case of spherically symmetric mass outflows, the mass-loss rate $\dot{M}$ is given by the continuity relation

$$\dot{M} = 4\pi R^2 \rho(R)\, v(R), \qquad (2)$$

where R is the radial distance from the center of the star, and $\rho(R)$ and $v(R)$ are the density and outflow speed at R, respectively. If one applies the density constraints provided by equilibrium thermodynamics discussed above to equation (2), the predicted mass-loss rates are far in excess of the maximum observed mass-loss rates for carbon stars (a few 10^{-4} $M_\odot$ /y). As noted above, C/O ~ 1.1 for CV stars requires that the pressure $P \gtrsim 3$ dynes/cm^2 in the stellar atmosphere for TiC to condense before graphite. For outflow speeds in grain formation regions (typically at radii $R \sim 3$ A.U.) that are as little as 5% of terminal outflow speeds (~10 – 20 km/s) of AGB stars, equation (2) yields mass-loss rates $\dot{M}$ in excess of 10^{-3} $M_\odot$ /y.

As the above calculation shows, if we use the gas pressures demanded by equilibrium thermodynamics, the inferred mass-loss rate for *symmetrically* distributed circumstellar matter is simply too large. Alternatively, if we use gas pressures that would be consistent with the observed mass loss rates in (assumed) spherically symmetric mass outflows, it is impossible to produce grains nearly as large as observed for presolar condensates. Indeed, were it not for the fact that circumstellar grains of micron-sized graphite are available for study in the laboratory, one would probably infer that only submicron-sized graphite grains could be produced in spherically symmetric AGB outflows, and we would certainly not have predicted the occurrence of refractory carbides inside of them. Yet, such grains *do* exist, and we must account for them. The necessary resolution to this problem is that the mass outflows of the carbon stars responsible for presolar graphites that contain carbides must depart radically from spherical symmetry, perhaps in the form of clumps or jets with enhanced densities and pressures (Bernatowicz *et al*., 1996; 2005; Chigai *et al*., 2002). This inference is consistent with astronomical observations of carbon stars with the highest mass-loss rates, such as the nearest (and best studied) carbon star IRC +10216. Weigelt *et al.* (1998), using speckle-masking interferometry, showed that the mass outflow from this star is neither spherically symmetric nor homogeneous, but is highly fragmented. They concluded that IRC +10216 appears to be in a very advanced stage of its evolution, probably in a phase immediately preceding its departure from the AGB.

The outflow velocity fields in the AGB circumstellar environment that are derived from detailed dynamical models (e.g., Ivezic *et al.,* 1998), considered in conjunction with formation temperatures implied by equilibrium thermodynamics and radiative equilibrium in the outflow, imply that the time intervals available for the growth of graphite are relatively short, on the order of a few years (Bernatowicz *et al*., 2005). These short time intervals cannot produce circumstellar graphites of the sizes observed as presolar grains (~ 1 μm diameter in KFC1) in spherically symmetric outflows, even under the most ideal grow conditions (perfect sticking efficiency, no evaporation, no depletion of gas species contributing to grain growth). This again points to the origin of circumstellar graphite in highly evolved CV stars that have inhomogeneous and clumpy mass outflows with enhanced densities and gas pressures.

5. GRAPHITE FROM SUPERNOVAE

The physical and chemical properties of graphite spherules formed in SN ejecta are quite different from those of spherules originating around AGB stars. The distinctions seem, at least in part, to reflect the disparities in hydrodynamics, in pressures, in gas compositions and in grain-formation timescales in the two environments. Although dust condensation in SN ejecta has been unambiguously observed (Meikle *et al*., 1993; Roche *et al*., 1993; Wooden *et al*., 1993; McCray, 1993), only limited inferences can be drawn from the astronomical observations regarding the composition and physical characteristics of the dust. Silicate formation has been inferred in various spectra from SN remnants (e.g., Arendt *et al*., 1999). Unfortunately, SN 1987A, which provided the best evidence for dust condensation in core-collapse SN, had a featureless spectrum with no evidence of silicate or SiC formation. This spectrum is consistent with the condensation of graphite and/or iron grains (Wooden, 1997), but the identification is tenuous because of the featureless nature of the IR spectra of these minerals. In general, IR astronomy can determine when and where dust has formed around SN, but is limited in its ability to characterize SN dust in terms of its mineralogy, chemical composition, or size. Given these limitations, the isotopic, chemical, and mineralogical studies of SN dust grains in the laboratory presently provide an alternative and exquisitely detailed source of information on grain formation in SN ejecta.

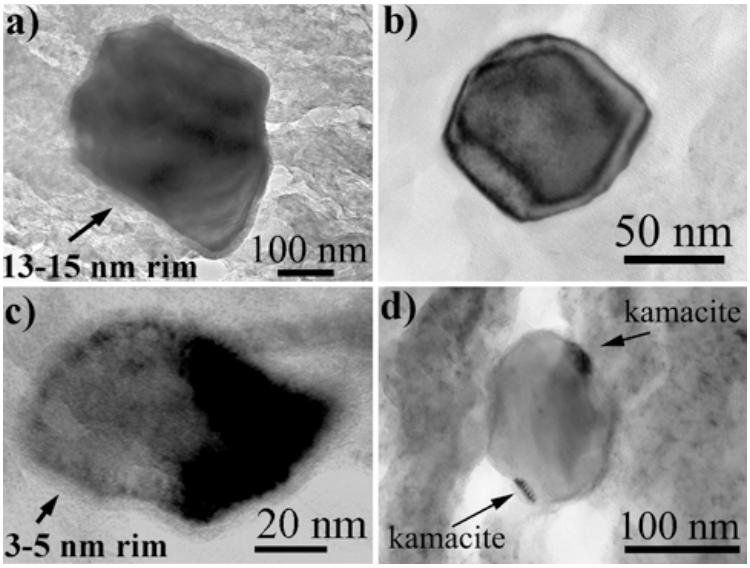

Figure 8. TEM bright field images of internal grains in supernova graphites from Murchison graphite separate KE3 (Amari *et al*., 1995b): a) TiC with an amorphous rim from spherule KE3e10; (b) euhedral TiC crystal from KE3e6 (the light and dark bands are thickness fringes); c) kamacite grain with an amorphous rim from spherule KE3d8 (Bernatowicz *et al.,* 1999); (d) subhedral TiC from KE3e6 with epitaxial kamacites on opposite (111) TiC faces. From Croat *et al*. (2003).

Low-density graphite spherules from density separate KE3 (1.65 - 1.72 g cm^{-3}) of the Murchison meteorite often have large excesses in ^{18}O and ^{28}Si, indicative of a supernova origin (Amari *et al*., 1995a). TEM examination of ultramicrotome sections of these SN graphites (Bernatowicz *et al*., 1998; 1999; Croat *et al*., 2003) reveal concentric turbostratic layers with a degree of graphitization intermediate between the onion and cauliflower types of graphite from AGB stars. The KE3 SN graphites are generally larger (4 – 12 μm) than the KFC1 graphites from carbon stars and have high abundances (25 - 2400 ppm) of internal TiC crystals (Figures 8a, 8b), with a single graphite in some cases containing hundreds of them. The TiC size

distributions among SN graphites are quite variable, with the geometrical mean TiC size ranging from 30 to 230 nm. Some, despite having similar total TiC abundances, have very different grain size distributions, and there is no obvious scaling relationship between the size of the graphite and the mean size of its internal grains.

Composite TiCs with iron-nickel subgrains, and solitary kamacite grains are also found in KE3 graphites (Figures 8c, 8d). In the composite grains, the iron phases are kamacite (0-24 at. % Ni) and taenite (up to 60 at. % Ni) epitaxially grown onto one or more TiC faces. This is direct, unambiguous evidence of Fe condensation in SN ejecta. The chemical variations among internal TiC grains (see below), as well as the presence of epitaxial Fe phases on some TiCs clearly indicate that the phase condensation sequence was TiC, followed by the iron phases (only found in some KE3 graphites) and finally graphite. Since graphite typically condenses at a higher temperature than iron at low pressures ($< 10^{-3}$ bars) in a gas with C > O and otherwise solar composition, the observed condensation sequence implies a relative iron enrichment in the gas or greater supersaturation of graphite relative to iron.

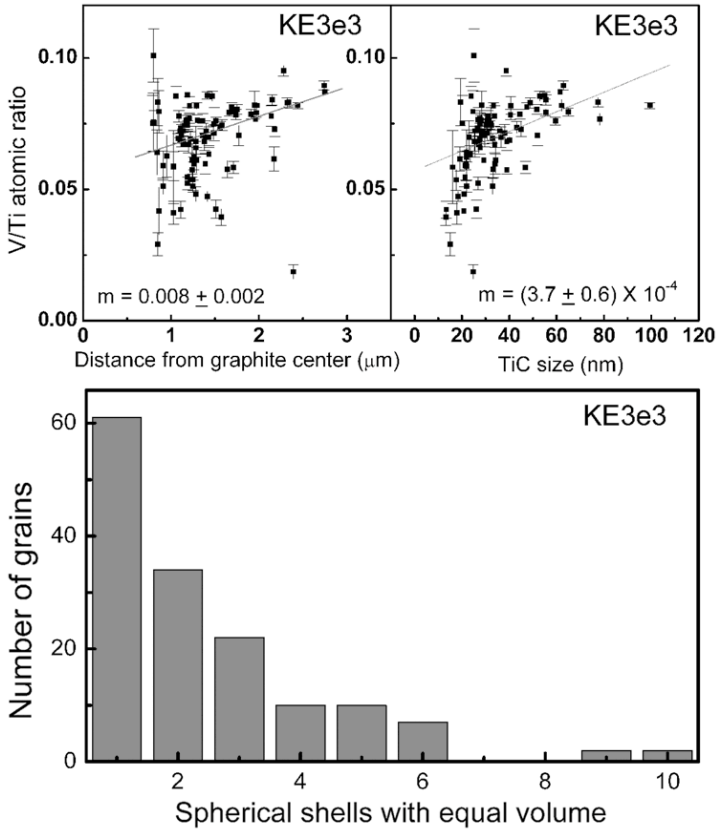

Figure 9. Trends of internal TiC crystals in supernova graphite spherule KE3e3 from Murchison. Upper panel: V/Ti atomic ratios as a function of three-dimensional radial distance from the spherule center, and as a function of TiC grain size. Slopes obtained from linear least-squares fits to the data are indicated. Lower panel: TiC number density in ten successive spherical shells of equal volume, starting at the graphite center. From Croat *et al*. (2003).

Examination of multiple ultramicrotome sections of each large spherule permits a determination of three-dimensional radial distances of internal crystals from the spherule center (based on the location of the crystal within the section and the section diameter). Since these radial distances are a rough measure of the time at which the internal grain was incorporated into

the graphite, temporal trends in various chemical and physical properties of grains in the ejecta can sometimes be discerned. Figure 9 shows the V/Ti atomic ratio *vs*. the radial distance from the graphite center in spherule KE3e3, for roughly 150 TiCs. Clear increases in the V/Ti ratio *vs*. radial distance are evident. This trend, also seen in other KE3 graphites, is probably due to chemical evolution of the TiCs in the ambient gas with time. Vanadium carbide, although soluble in TiC, is less refractory and condenses at a substantially lower temperature (cf. Lodders and Fegley, 1995). Thus, TiCs found towards the graphite exterior, which were probably exposed to the gas for longer times and at lower temperatures prior to capture by the graphite, incorporated more V. The observed trend in V/Ti suggests that this ratio was continually evolving in the TiCs before they were incorporated into the graphite, but ceased evolving once the TiC was fully encased.

There is typically a decrease in the number density of internal grains as a function of increasing radial distance (therefore later graphite condensation times) from the SN graphite centers. This is shown in Figure 9, in which the volume of graphite spherule KE3e3 has been subdivided into ten spherical shells of equal volume, with the number of TiCs counted in each shell. The number of internal TiCs is clearly higher in the central shells than in the outermost ones. If the TiCs already present in the gas were accreted onto growing graphite spherules, the mechanism of their capture is essentially the same as that of the carbon-bearing molecules contributing to graphite growth. That the relative numbers of molecules and TiCs captured in a given time interval is not constant requires a change either in their relative abundance or in their relative sticking probabilities. One possibility is a progressive increase in the effective sticking probability of carbon-bearing molecules onto graphite, relative to TiC, over the time of graphite growth. This is most simply explained if we assume that the sticking probability of the molecules contributing to graphite growth increases with decreasing ambient temperature, resulting in a smaller number density of TiCs in graphite at greater spherule radii. Alternatively, the relative abundance of TiCs in the gas could have decreased over time if the TiCs had a substantially higher sticking probability than carbon-bearing molecules, and were more rapidly depleted from the gas.

TiC morphologies reflect variable degrees of "weathering" in the SN outflow. Most TiCs (about 90%) are euhedral to subhedral, with primary growth faces somewhat corroded but still clearly defined (Figure 8b). Some KE3 TiCs are surrounded by an amorphous or nearly amorphous rim layer 3-15 nm thick, partially or completely enveloping the grain (Figure 8a). Rims have also been observed on metal grains in KE3 graphite (Fig. 8c). Rimmed grains are ubiquitous, and constitute up to nearly half of the TiC population in some graphites. The partially amorphous rims (3 – 15 nm) seen on both TiC and kamacite grains are comparably thick and related in composition to their host grains (Bernatowicz *et al*., 1999). Given these observations, at least two grain alteration mechanisms may be conceived: particle irradiation and chemical corrosion. The rims resemble the solar-wind damage features seen on lunar soil grains, which have ~50 nm thick amorphous rims caused by irradiation with ~1 keV/nucleon (≈400 km/s) H and He ions (cf. Keller and McKay, 1997). TiCs and kamacite grains forming in SN ejecta may also have been exposed to particle irradiation, a kind of "reverse solar wind," due to collisions between the grains and slower-moving parcels of gas. Fingers of gas are ejected at high velocities (~10^4 km/s) in SN due to Rayleigh-Taylor instabilities (Wooden, 1997). In such an environment, a drift velocity $\Delta v \sim 100$ km/s between the grains and slower-moving parcels of gas is plausible, being at most only a few percent of the mass outflow speed. A drift velocity of

this magnitude is a factor of several less than the solar wind speed, and so damaged regions less thick (~10 nm) than those observed on lunar grains are reasonable.

Alternatively, damaged rims could result from chemical corrosion, provided that gas conditions were to change with time to a state in which the TiCs and kamacites were no longer stable. However, this seems less likely given that comparably thick rims are found on compositionally dissimilar phases. Moreover, in the case of KE3e3, where ≤ 6% of the TiCs have rims, the TiC size *vs*. radial distance trends (Figure 9) indicate that most of the TiCs were still growing at the time they were incorporated into their host graphite, so the gas environment could not be simultaneously corroding and growing TiCs. In general, the diversity in TiC properties suggests that TiCs formed first and had substantially diverse histories prior to incorporation into the graphite, implying some degree of turbulent mixing in the SN outflows.

The TEM observations allow inferences to be made about the typical physical conditions in the SN ejecta where the grains condensed. Given the TiC sizes and abundances, the gas was evidently quite dusty. From the observed range in TiC sizes of ~20 nm to ~500 nm, the *minimum* Ti number densities in the gas (assuming ~1 year growth time and T ≤ 1800°K) are inferred to be ~7 x 10^4 to ~2 x 10^6 atoms/ cm^3, respectively. Although the gas composition is clearly *not* solar, for scale, these number densities would correspond to a range in total pressure from ~0.2 dynes/cm^2 to ~5.0 dynes/cm^2 in a gas of solar composition. They also correspond to minimum TiC grain number densities of ~3 x 10^{-4} to ~0.2 grains/cm^3, assuming complete condensation of Ti in TiC. The TiC number densities imply a maximum average ratio of TiC grain separation distance in the gas to grain diameter of ~3 x 10^5 to ~1 x 10^6 (Croat *et al*., 2003).

In contrast to the Murchison KFC1 graphites, Zr- Ru- Mo-carbides are *not* observed in SN graphites. This is independent evidence that the weak s-process, from $^{22}Ne(\alpha,n)^{25}Mg$ in the helium burning cores of stars massive enough to form SN, does not give rise to large enough neutron exposures to elevate the abundances of these elements to anything close the levels seen in the carbides from AGB stars (see Meyer and Zinner, 2005).

6. METEORITIC NANODIAMONDS

The most abundant refractory carbonaceous mineral in chondrites is nanometer-sized diamond. Nanodiamonds were first isolated from chondrites by destructive chemical dissolution of meteorite matrices (Lewis *et al*., 1987). The bulk C isotopic compositions of nanodiamond separates measured by stepped combustion of acid dissolution residues of various carbonaceous, ordinary, and enstatite chondrites are all close to the solar mean, with $\delta^{13}C$ = -32.5 to -38.8 per mil (Russell *et al*., 1996). Although the mean C isotopic composition of nanodiamonds is essentially solar, there is sufficient isotopic evidence implying that at least *some* meteoritic nanodiamonds are of presolar origin. Nanodiamond separates from acid dissolution residues of chondrites are linked to various isotopic anomalies in H (Virag *et al*., 1989), N (Arden *et al*., 1989; Russell *et al*., 1991; 1996), Sr (Lewis *et al*., 1991), Pd (Mass *et al*., 2001), Te (Richter *et al*., 1997; Mass *et al*., 2001), Xe (Lewis *et al*., 1987), and Ba (Lewis *et al*., 1991). However, only the anomalous Xe and Te associated with SN provide tenable evidence for a presolar origin for at least a subpopulation of the diamonds (Zinner, 2004; Daulton, 2005). Definitive isotopic evidence of a presolar origin for all or part of the population remains elusive because of the extremely small size of the diamonds. Meteoritic nanodiamonds have effective diameters, defined as the square root of their TEM projected cross-sectional areas, that range between 0.1 and 10 nm with a median of the distribution of 2.58 nm and 2.84 nm for diamonds isolated from

the Murchison and Allende carbonaceous chondrites, respectively (Daulton *et al.,* 1996). This is consistent with earlier, indirect and lower spatial-resolution size measurements by TEM (Lewis *et al.,* 1989; Fraundorf *et al.,* 1989).

The smallest mineral grains that can be analyzed isotopically by the most advanced generation of secondary ion mass spectrometry (SIMS) instruments, the NanoSIMS, are ~ 0.1 μm. This is several orders of magnitude larger than meteoritic nanodiamonds. Presently, there are no instruments capable of measuring the isotopic compositions of an individual nanocrystal. In fact, even if there were, the only element in an individual nanodiamond whose isotopic composition could be feasibly measured is that of the primary element C. For example, an average meteoritic nanodiamond contains a mere several thousand C atoms (between 1.0×10^3 - 7.5×10^3) and only tens of N atoms (< 100), where N is the second most abundant trapped element (1800-13000 ppm by mass; Russell *et al.*, 1996) following surface bound H (10-40 at.%; Virag *et al.*, 1989). Since there is only one trapped noble gas atom per tens of average-sized meteoritic nanodiamonds, measurement of isotopic compositions of trapped noble gases in individual meteoritic nanodiamonds is impossible. The situation is more extreme for isotopically anomalous Xe and Te, for which there is only one trapped Xe or Te atom per millions of mean-sized meteoritic nanodiamonds (see Zinner, 2004; Daulton, 2005). Consequently, all isotopic measurements of meteoritic nanodiamonds are of elements/gases extracted from billions of individual diamonds. In sharp contrast, the other known presolar minerals are submicron to micron in size and large enough that isotopic measurements can be performed on individual grains. The origin of meteoritic nanodiamond thus remains largely enigmatic because of its grain size.

Several hypotheses have been put forth for the origin of meteoritic nanodiamonds. Supernovae have been suggested as a source based on the inseparable presence of isotopically anomalous Xe (termed Xe-HL; Lewis *et al.*, 1987) of probable SN origin, indicating some meteoritic nanodiamonds formed in, or at least were associated with, SN. However, the high abundance of nanodiamonds in chondrites (matrix normalized ~1400 ppm in Murchison; Huss, 1997) suggests a prolific dust source. Although SN are the major contributors of gaseous matter in the ISM, they are not the dominant source of condensed matter. This has led to the suggestion that AGB stars or even the solar nebula are dominant sources. The latter is consistent with normal bulk C isotopic composition of meteoritic nanodiamonds. In fact, Dai *et al.* (2002) interpreted the presence of nanodiamonds in IDPs *conjectured* to originate from asteroids, and their absence in IDPs *conjectured* to originate from comets, as a possible argument for nanodiamond formation in the inner solar system. Alternatively, the ensemble average of a myriad of nanodiamonds from a wide variety of stellar sources may simply mirror the solar mean.

A number of mechanisms have been proposed for nanodiamond formation in SN, these include: formation by low-pressure condensation, similar to chemical vapor deposition (CVD), in expanding gas ejecta (Clayton *et al.,* 1995); shock metamorphism of graphite or amorphous-carbon grains in the ISM driven by high-velocity (grain impact grain) collisions in SN shock waves (Tielens *et al.,* 1987); annealing of graphite particles by intense ultraviolet radiation (Nuth and Allen, 1992); and irradiation-induced transformation of carbonaceous grains by energetic ions (Ozima and Mochizuki, 1993). Condensation by CVD mechanisms in circumstellar atmospheres of carbon stars has been proposed (Lewis *et al.*, 1987). Nanodiamond formation in the solar nebula, (Dai *et al.*, 2002) presumably by CVD, has also been proposed.

Microstructures of materials are heavily dependent on growth mechanisms, physical conditions during formation, and post-formation alteration mechanisms. Therefore, to evaluate several of the formation theories for meteoritic nanodiamonds, Daulton *et al.* (1996) used HR-TEM to compare nanodiamonds synthesized by shock metamorphism (Greiner *et al.,* 1988) and CVD (Frenklach *et al.,* 1991) to those isolated from the Allende and Murchison carbonaceous chondrites. Although changes in experimental conditions can result in a range of growth features and affect the proportion of nanodiamonds synthesized by any given process, microstructural features should exist that are uniquely characteristic of specific formation mechanisms exclusive to either condensation or shock metamorphism. In fact, such features were identified in the synthesized nanodiamonds, and when compared to the microstructures of nanodiamonds from Allende and Murchison, they indicated that the predominant mechanism for meteoritic nanodiamond formation is vapor condensation. The results of the Daulton *et al.* (1996) study represent the only detailed microstructural data on meteoritic nanodiamonds to date, and are summarized here.

Table 1: Nanodiamond Microstructures

	Shock	Meteoritic	CVD
Twins / Single-Crystals	2.48	1.28	1.25
Linear Twins / Non-Linear Twins	2.72	0.87	0.36
Star Twins / All Twins	0.04	0.09	0.23
Dislocations	yes	no [a]	no [a]

[a] Not observed

In cubic diamond, twinning along {111} planes is common and results when the stacking sequence of {111} planes is abruptly reversed, e.g. {*AaBbCcBbAa*}. In coincident site lattice notation, this twin structure is described as a first order Σ=3 {111} twin. The interface at a Σ=3 twin boundary is one of the lowest-energy lattice defects, so cubic nanocrystals can form Σ=3 twin structures relatively easily to accommodate growth constraints. Thus, Σ=3 twin microstructures can provide a diagnostic indicator for different nanodiamond formation mechanisms.

Multiple Σ=3 twins are relatively common microstructures in nanodiamonds and occur in two configurations. The first type (linear) exhibits parallel Σ=3 {111} twin boundaries that terminate at the crystal surface (Figure 10). The second type (non-linear) is characterized by oblique Σ=3 {111} twin boundaries that terminate either at crystal surfaces, twin boundary intersections, or both (Figure 10). Important differences become apparent when the relative abundances of twin microstructures are compared in the synthesized diamonds (Figure 11). Firstly, the ratio of twinned crystals to single crystals in shock-synthesized diamonds (2.48; Table 1) is a factor of two higher than for those synthesized by CVD (1.25). Since re-entrant corners of twinned crystals are associated with increased growth rates over single crystals (Angus *et al.,* 1992), this suggests that the mean growth rate for shock-synthesized diamonds is greater than the mean growth rate of CVD-synthesized diamonds. Nanodiamonds synthesized by detonation must have experienced rapid thermal quenching to escape graphitization after the passage of the shock front. Those nanodiamonds that survived must have experienced high growth rates. The ratio of single crystals to twinned crystals in the meteoritic nanodiamonds (1.28; Table 1) suggests growth rates similar to those of the CVD-synthesized diamonds.

Secondly, linear twins dominate over non-linear twins in shock-synthesized nanodiamonds. During detonation synthesis of nanodiamonds, large, highly anisotropic shock pressure gradients would momentarily exist. Following a shock-induced carbonaceous grain-on-grain collision, partially molten material would rapidly solidify behind planar shock fronts. Further, any potential nanodiamond condensation at high-pressure shock fronts would occur within highly anisotropic conditions. In both cases, crystallization should occur along planar growth fronts producing microstructures dominated by parallel twin boundaries. Consistent with this interpretation, the shock-synthesized nanodiamonds display a distribution of multiple twins dominated by parallel twin boundaries. The direction of growth is presumably related to the geometry of the shock front and direction of the pressure gradients. In sharp contrast, the CVD-synthesized nanodiamonds are dominated by non-linear multiple twins indicative of isotropic growth. The multiply twinned structures of meteoritic nanodiamonds more closely resemble CVD nanodiamonds.

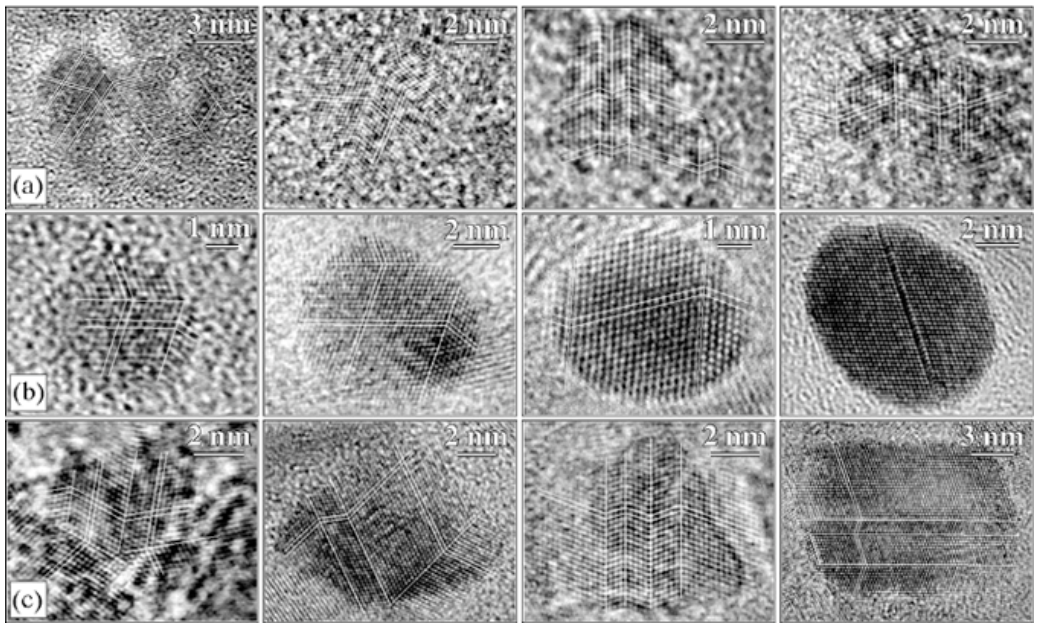

Figure 10. Multiply-twinned microstructures in meteoritic (row a), CVD (row b), and detonation (row c) nanodiamonds. The two columns to the left are non-linear multiple twins and the two columns to the right are linear multiple twins.

The most striking non-linear, multiply-twinned configurations correspond to symmetric multiply-twinned particles (MTPs). Nanodiamonds synthesized by direct nucleation and homoepitaxial growth from the vapor phase have a large abundance of decahedra MTPs which have pseudo-five-fold or star morphology (Figure 12). Similar to CVD nanodiamonds, star twins are relatively common growth features in the meteoritic nanodiamonds. In contrast, star twins are relatively rare in shock synthesized nanodiamonds with an abundance at least a factor of two less than meteoritic nanodiamonds (Figure 11). The coherent twin boundaries present in the star twins are indicative of radial (isotropic) growth as would be possible from the direct nucleation and homoepitaxial growth from a locally uniform supersaturated gas such as in a CVD-type process. Star-twin microstructures would not be expected from the highly anisotropic shock-induced metamorphism of carbonaceous grains. The non-linear multiple-twin crystals (including MTPs) observed in detonation soot residues might have formed by a less efficient

mechanism occurring within the rarefaction wave of the expanding shock front. Vaporization of a fraction of the precursor carbonaceous material in the shock heating event could supersaturate the partially ionized gas in C. Given favorable conditions, vapor condensation might occur after the passage of the shock front leading to nanodiamond nucleation and growth.

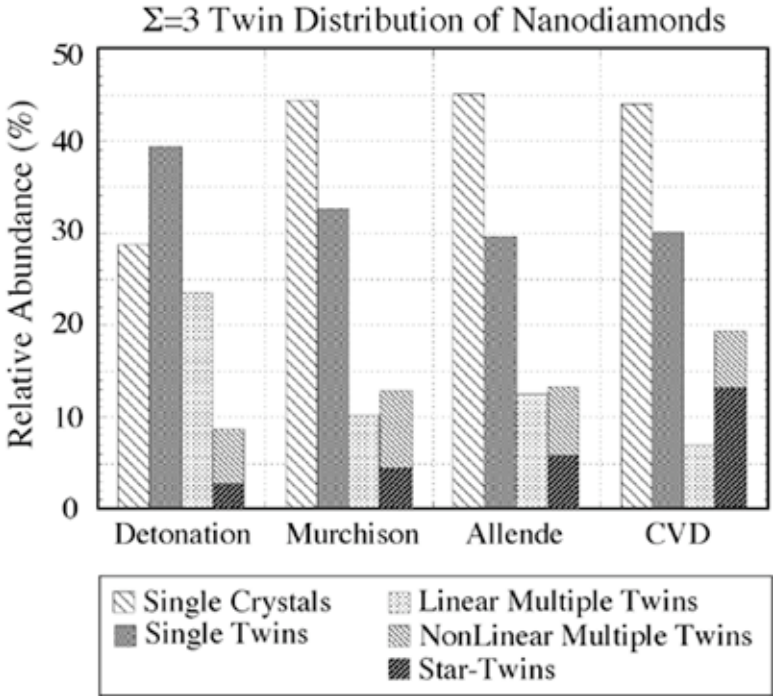

Figure 11. Normalized distribution of Σ=3 twin microstructures for nanodiamonds synthesized by detonation shock (Greiner *et al.,* 1988) and CVD (Frenklach *et al.,* 1991) as well as those isolated from the chondrites Murchison and Allende. Unobstructed and isolated nanodiamonds exhibiting clear cross-lattice fringes were classified by their twin type. Statistics are based on 209 (detonation), 372 (Murchison), 257 (Allende), and 130 (CVD) individual nanodiamonds; a total of 968 nanodiamonds.

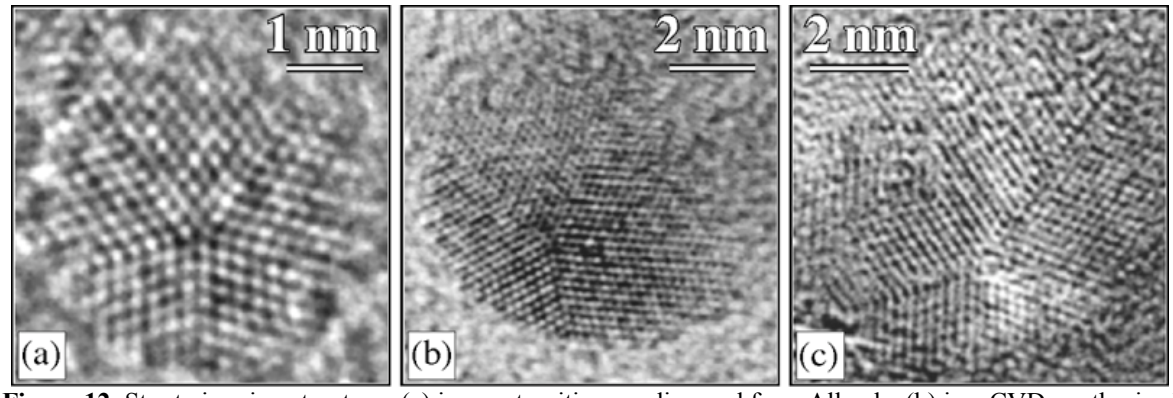

Figure 12. Star twin microstructures (a) in a meteoritic nanodiamond from Allende, (b) in a CVD-synthesized nanodiamond, and (c) in a shock-synthesized nanodiamond.

In contrast to twin and stacking faults structures, dislocations represent relatively high-energy defects because their cores contain disrupted nearest-neighbor bonds and significant bond distortion. Whereas the formation of twins and stacking faults is influenced by low-energy processes, the formation of dislocations requires relatively high-energy processes. This is

especially the case for diamond, which has strong sp^3 carbon bonds. For example, epitaxial dislocations are common in CVD diamond films and result from strain induced at the substrate interface and at interfaces where two growing crystals impinge at an arbitrary angle. High dislocation densities also develop in natural diamond to accommodate lattice distortions around mineral inclusions and plastic deformation caused by shear stresses in the earth's upper mantle. In contrast, the situation is disparate for nanocrystals, where perhaps only a few mechanisms are available to form high-energy defects. Martensitic-type mechanisms occurring behind shock fronts can leave a high density of residual dislocation defects in the transformation product (Daulton *et al.*, 1996). Shock synthesized nanodiamonds exhibit a small population of grains that contain dislocations with disorder (Figure 13). In contrast, dislocations are not expected to form in nanometer grains that nucleated directly from the vapor phase, and indeed, no such defect structures were observed in the CVD-synthesized nanodiamonds.

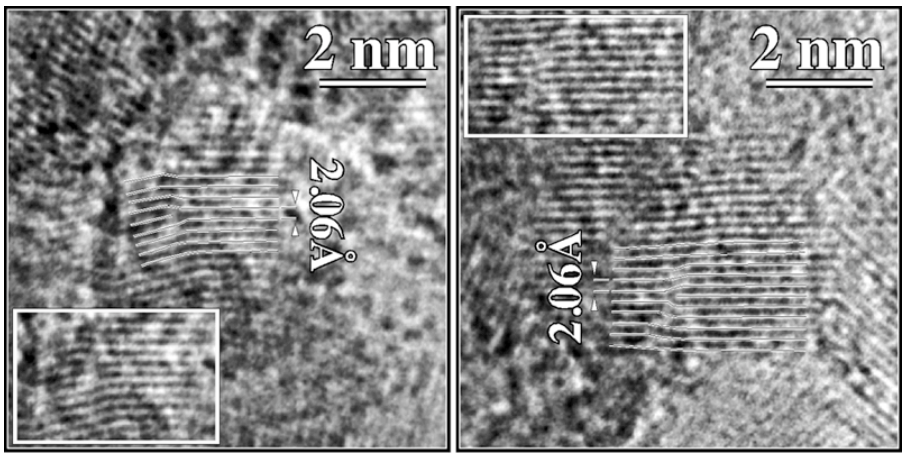

Figure 13. Shock-synthesized nanodiamonds containing dislocations. The superimposed lines illustrate the missing <111> half planes. Insets display non-annotated dislocation images.

No analogous dislocations were observed in the Allende and Murchison nanodiamonds. It is unlikely that the acid dissolution used to isolate meteoritic nanodiamonds destroyed those with dislocations. Detonation soot residues were subjected to acid treatments to purify diamond products (Greiner *et al.,* 1988), although not as extensive as the treatments used to isolate nanodiamonds from chondrites. Nevertheless, the detonation soot residues still retain nanodiamonds with dislocations. Furthermore, thermal processing of the Murchison and Allende parent bodies was probably insufficient to remove dislocations by annealing or destroying dislocation-containing diamonds. Noble gas abundances in nanodiamonds suggest mild thermal processing in Murchison with only minimal loss of nanodiamonds (Huss and Lewis, 1995). Although Allende experienced greater thermal processing than Murchison, a significant amount of surface-bound H with deuterium excesses is retained by its nanodiamonds (Carey *et al.,* 1987; Virag *et al.,* 1989). Temperatures required to anneal dislocations would be more than sufficient to desorb surface hydrogen, resulting in a significant depletion of any deuterium excess. Lack of dislocation microstructures in meteoritic nanodiamonds is probably a primary feature of formation, and therefore suggests that the majority of meteoritic nanodiamonds did not form by shock metamorphism.

Microstructures of nanodiamonds isolated from Allende and Murchison, for the most part, are similar to those of CVD-synthesized nanodiamonds and dissimilar from those of the shock-

synthesized nanodiamonds (Table 1). Twin microstructures of meteoritic nanodiamonds suggest isotropic growth conditions, and the lack of dislocations is inconsistent with shock processes. These observations suggest that the predominant mechanism responsible for the formation of meteoritic nanodiamonds is low-pressure condensation, similar to CVD. This conclusion is based on direct microstructural evidence, independent of any models for astrophysical processes or environments (e.g., AGB stars, SN, or the solar nebula). If shock metamorphism (most probably occurring in SN) contributed to the population of nanodiamonds in meteorites, then certainly shock-formed nanodiamonds represent a minor subpopulation, since the majority of the meteoritic nanodiamonds do not exhibit microstructures indicative of anisotropic shock.

ACKNOWLEDGEMENTS

This chapter is based upon work partially supported by NASA under contracts NNG04GG13G (TJB, TKC) and W-10246 (TLD), issued through the Office of Space Science and NRL through the Office of Naval Research (TLD).

REFERENCES

Alexander C. M. O'D., Swan P., and Walker R. M. (1990) In situ measurement of interstellar silicon carbide in two CM chondrite meteorites. *Nature* **348**, 715-717.

Amari S., Lewis R. S., and Anders E. (1994) Interstellar grains in meteorites: I. Isolation of SiC, graphite, and diamond; size distributions of SiC and graphite. *Geochim. Cosmochim. Acta* **58**, 459-470.

Amari S., Zinner E., and Lewis R. S. (1995a) Large ^{18}O excesses in circumstellar graphite grains from the Murchison meteorite: Indication of a massive-star origin. *Astrophys. J.* **447**, L147-150.

Amari S., Lewis R. S., and Anders E. (1995b) Interstellar grains in meteorites: III. Graphite and its noble gases. *Geochim. Cosmochim. Acta* **59**, 1411-1426.

Amari S., Nittler L. R., Zinner E., Gallino R., Lugaro M., and Lewis R. (2001) Presolar SiC grains of type Y: Origin from low metallicity asymptotic giant branch stars. *Astrophys. J.* **546**, 248-266.

Amari S., Zinner E., and Lewis R. S. (2004) Isotopic study of presolar graphite in the KFC1 separate from the Murchison meteorite. *Meteorit. Planet. Sci.* **39**, A13.

Angus J. C., Sunkara M., Sahaida S. R., and Glass J. T. (1992) Twinning and faceting in early stages of diamond growth by chemical vapor deposition. *J. Mat. Research* **7**, 3001-3009.

Arden J. W., Ash R. D., Grady M. M., Wright I. P., and Pillinger C. T. (1989) Further studies on the isotopic composition of interstellar grains in Allende: 1. Diamonds. *Lunar Planet. Sci.* **XX**, 21-22 .

Arendt R. G., Dwek E., and Moseley S. H. (1999) Newly synthesized elements and pristine dust in the Cassiopeia A supernova remnant. *Astrophys. J.* **521**, 234-245.

Bennett C. L., Halpern M., Hinshaw G., Jarosik N., Kogut A., Limon M., Meyer S. S., Page L., Spergel D. N., Tucker G. S., Wollack E., Wright E. L., Barnes C., Greason M. R., Hill R. S., Komatsu E., Nolta M. R., Odegard N., Peiris H. V., and Weiland J. L. (2003) First year Wilkinson Microwave Anisotropy Probe (WMAP) observations: Preliminary maps and basic results. *Astrophy. J. Suppl. Ser.* **148**, 1-27.

Bergeat J., Knapik A., and Rutily B. (2001) The effective temperatures of carbon-rich stars. *Astron. Astrophy.* **369**, 178-209.

Bergeat J., Knapik A., and Rutily B. (2002a) Carbon-rich giants in the HR diagram and their luminosity function. *Astron. Astrophy.* **390**, 967-986.

Bergeat J., Knapik A., and Rutily B. (2002b) The pulsation modes and masses of carbon-rich long period variables. *Astron. Astrophy.* **390**, 987-999.
Bernatowicz T. J. and Walker R. M. (1997) Ancient stardust in the Laboratory. *Physics Today*, **50 No. 12**, 26-32.
Bernatowicz T. J. and Zinner E., Eds. (1997) *Astrophysical Implications of the Laboratory Study of Presolar Materials*, AIP, New York, 750 pp.
Bernatowicz T. J., Amari S., Zinner E. K., and Lewis R. S. (1991) Interstellar grains within interstellar grains. *Astrophys. J.* **373**, L73-L76.
Bernatowicz T. J., Cowsik R., Gibbons P., Lodders K., Fegley B., Amari S., and Lewis R. (1996) Constraints on stellar grain formation from presolar graphite in the Murchison meteorite. *Astrophys. J.* **472**, 760-782.
Bernatowicz T. J., Amari S., Messenger S., and Lewis R. (1998) Internal structure and composition of presolar graphites from supernovae. *Lunar Planet. Sci.* ***XXIX***. Abstract #1393.
Bernatowicz T. J., Bradley J., Amari S., Messenger S., and Lewis R. (1999) New kinds of massive star condensates in a presolar graphite from Murchison. *Lunar Planet. Sci.* ***XXX***, Abstract #1392.
Bernatowicz T. J., Messenger S., Pravdivtseva O., Swan P., and Walker R. M. (2003) Pristine presolar silicon carbide. *Geochim. Cosmochim. Acta* **67**, 4679-4691.
Bernatowicz T. J., Akande O. W., Croat T. K., and Cowsik R. (2005) Constraints on grain formation around carbon stars from laboratory studies of presolar graphite. *Lunar Planet. Sci.* **XXXVI**, Abstract #1509.
Bowen G. H. (1988) Dynamical modeling of long-period variable star atmospheres. *Astrophys. J.* **329**, 299-317.
Carey W., Zinner E., Fraundorf P., and Lewis R. S. (1987) Ion probe and TEM studies of a diamond bearing Allende residue. *Meteoritics* **22**, 349-350.
Chigai T., Yamamoto T., and Kozasa T. (2002) Heterogeneous condensation of presolar titanium carbide core-graphite mantle spherules. *Meteorit. Planet. Sci.*, **37**, 1937-1951.
Clayton D. D. and Nittler L. R. (2004) Astrophysics with Presolar Stardust**.** *Ann. Rev. Astron. Astro.* **42**, 39-78.
Clayton D. D., Meyer B. S., Sanderson C. I., Russell S. S., and Pillinger C. T. (1995) Carbon and nitrogen isotopes in type II supernova diamonds. *Astrophys. J.* **447**, 894-905.
Croat T. K., Bernatowicz T., Amari S., Messenger S., and Stadermann F. J. (2003) Structural, chemical and isotopic microanalytical investigations of graphite from supernovae. *Geochim. Cosmochim. Acta* **67**, 4705-4725.
Croat T. K., Stadermann F. J., Zinner E., and Bernatowicz T. J. (2004) Coordinated Isotopic and TEM Studies of Presolar Graphites from Murchison. *Lunar Planet. Sci.* **XXXV**, Abstract #1353.
Croat T. K., Stadermann F. J., and Bernatowicz T. J. (2005a) Internal grains within KFC graphites: Implications for their stellar source. *Lunar Planet. Sci.* **XXXVI**, Abstract #1507.
Croat T. K., Stadermann F. J., and Bernatowicz T. J. (2005b) Presolar Graphite From AGB stars: microstructure and s-process enrichment. *Astrophys. J.* In press.
Dai Z. R., Bradley J. P., Joswiak D. J., Brownlee D. E., Hill H. G. M., and Genge M. J. (2002) Possible *in situ* formation of meteoritic nanodiamonds in the early solar system. *Nature* **418**, 157-159.
Daulton T. L. (2005) Nanodiamonds in the Cosmos. Microstructural and trapped element isotopic data. In *Syntheses, Properties, and Applications of Ultrananocrystalline Diamond* (eds. D. M. Gruen, O. A. Shenderova, and A. Y. Vul'), Springer, pp. 49 – 62.
Daulton T. L., Eisenhour D. D., Bernatowicz T. J., Lewis R. S., and Buseck P. R. (1996) Genesis of presolar diamonds: Comparative high-resolution transmission electron microscopy study of meteoritic and terrestrial nano-diamonds. *Geochim. Cosmochim. Acta* **60**, 4853-4872.
Daulton T. L., Bernatowicz T. J., Lewis R. S., Messenger S., Stadermann F. J., and Amari S. (2002) Polytype distribution in circumstellar silicon carbide. *Science* **296**, 1852-1855.

Daulton T. L., Bernatowicz T. J., Lewis R. S., Messenger S., Stadermann F. J., and Amari S. (2003) Polytype distribution in circumstellar silicon carbide: Microstructural characterization by transmission electron microscopy. *Geochim. Cosmochim. Acta* **67**, 4743-4767.

ESA (1997) *The HIPPARCHOS Catalog*, ESA SP-1200, ESA, Netherlands.

Forrest W. J., Gillett F. C., and Stein W. A. (1975) Circumstellar grains and the intrinsic polarization of starlight. *Astrophys. J.* **195**, 423-440.

Fraundorf P., Fraundorf G., Bernatowicz T., Lewis R., and Tang M. (1989) Stardust in the TEM. *Ultramicroscopy* **27**, 401-412.

Fraundorf P. and Wackenhut M. (2002) The core structure of presolar graphite onions. *Astrophys. J.* **578**, L153-L156.

Frenklach M., Howard W., Huang D., Yuan J., Spear K. E., and Koba R. (1991) Induced nucleation of diamond powder. *Appl. Phy. Lett.* **59**, 546-548.

Gallino R., Busso M., and Lugaro M. (1997) Neutron capture nucleosynthesis in AGB stars. In *Astrophysical Implications of the Laboratory Study of Presolar Materials* (eds. T. J. Bernatowicz and E. Zinner), AIP, New York, 115-153.

Greiner N. R., Phillips D. S., Johnson J. D., and Volk F. (1988) Diamonds in detonation soot. *Nature* **333**, 440-442.

Habing H. J., Tignon J., and Tielens A. G. G. M. (1994) Calculations of the outflow velocity of envelopes of cool giants. *Astron. Astrophys.* **286**, 523-534.

Hoppe P. and Ott U. (1997) Mainstream silicon carbide grains from meteorites. In *Astrophysical Implications of the Laboratory Study of Presolar Materials* (eds. T. J. Bernatowicz and E. Zinner), AIP, New York, 27-58.

Huss G. R. (1997) The survival of presolar grains in solar system bodies. In *Astrophysical Implications of the Laboratory Study of Presolar Materials* (eds. T. J. Bernatowicz and E. Zinner), AIP, New York, 721-748.

Huss G. R. and Lewis R. S. (1995) Presolar diamond, SiC, and graphite in primitive chondrites: Abundances as a function of meteorite class and petrologic type. *Geochim. Cosmochim. Acta* **59**, 115-160.

Iben I. (1967) Stellar evolution. VI. Evolution from the main sequence to the Red-Giant branch for stars of mass 1 $M_{\odot}$, 1.25 $M_{\odot}$, and 1.5 $M_{\odot}$. *Astrophys. J.* **147**, 624-649.

Ivezic Z., Knapp G. R., and Elitzur M. (1998) Stellar outflows driven by radiation pressure. In *Proceedings of The Sixth Annual Conference of the CFD Society of Canada*, CFDSC, Ottawa IV-13.

Jones A. P., Tielens A. G. G. M., Hollenbach D. J., and McKee C. F. (1997) The propagation and survival of interstellar grains. In *Astrophysical Implications of the Laboratory Study of Presolar Materials* (eds. T. J. Bernatowicz and E. Zinner), AIP, New York, 595-613.

Keller L. P. and McKay D. S. (1997) The nature and origin of rims on lunar soil grains. *Geochim. Cosmochim. Acta* **61**, 2331-2341.

Krauss L. M. and Chaboyer B. (2003) Age estimates of globular clusters in the Milky Way: Constraints on cosmology. *Science* **299**, 65-69.

Lambert D. L., Gustafsson B., Eriksson K., and Hinkle K. H. (1986) The chemical compositions of carbon stars. I. Carbon, nitrogen, and oxygen in 30 cool carbon stars in the galactic disk. *Astrophys. J. Suppl.* **62**, 373-425.

Lampens P., Kovalevsky J., Froeschle M., and Ruymaekers G. (1997) On the mass-luminosity relation. In *Proceedings of the ESA Symposium "Hipparchos – Venice '97"*, ESA SP-402, ESA, Netherlands, 421-424.

Lattanzio J. C. and Boothroyd A. I. (1997) Nucleosynthesis of elements in low to intermediate mass stars through the AGB phase. In *Astrophysical Implications of the Laboratory Study of Presolar Materials* (eds. T. J. Bernatowicz and E. Zinner), AIP, New York, 85-114.

Lewis R. S., Tang M., Wacker J. F., Anders E., and Steel E. (1987) Interstellar diamonds in meteorites. *Nature* **326**, 160-162.

Lewis R. S., Anders E., and Draine B. T. (1989) Properties, detectability and origin of interstellar diamonds in meteorites. *Nature* **339**, 117-121.

Lewis R. S., Huss G. R., and Lugmair G. (1991) Finally, Ba & Sr accompanying Xe-HL in diamonds from Allende. *Lunar Planet. Science* **XXII**, 807-808.
Lodders K. and Fegley B. Jr. (1995) The origin of circumstellar silicon carbide grains found in meteorites. *Meteoritics* **30**, 661-678.
Lodders K. and Fegley B. Jr. (1997) Condensation chemistry of carbon stars. In *Astrophysical Implications of the Laboratory Study of Presolar Materials* (eds. T. J. Bernatowicz and E. Zinner), AIP, New York, 391-423.
Maas R., Loss R. D, Rosman K. J. R., De Laeter J. R., Lewis R. S., Huss G. R., and Lugmair G. W. (2001) Isotope anomalies in tellurium and palladium from Allende nanodiamonds. *Meteorit. Planet. Sci.* **36**, 849-858.
Martin C., Mignard F., Hartkopf W. I., and McAlister H. A. (1998) Mass determination of astrometric binaries with Hipparcos. *Astron. Astrophys. Suppl. Ser.* **133**, 149-162.
McCray R. (1993) Supernova 1987A revisited. *Ann. Rev. Astron. Astrophys.* **31**, 175-216.
McDonald J. E. (1963) Homogeneous nucleation of vapor condensation II: Kinetic aspects. *Am. J. Phys.* **31**, 31-41.
Meikle W. P. S, Spyromilio J., Allen D. A., Varani G. -F., and Cummings R. J. (1993) Spectroscopy of supernova 1987A at 1-4 □m –II. Days 377 to 1114. *MNRAS* **261**, 535-572.
Mendybaev R. A., Beckett J. R., Grossman L., Stolper E., Cooper R. F., and Bradley J. P. (2002) Volatilization kinetics of silicon carbide in reducing gases: An experimental study with applications to the survival of presolar grains in the solar nebula. *Geochim. Cosmochim. Acta* **66**, 661-682.
Messenger S., Amari S., Gao X., Walker R. M., Clemett S. J., Chillier X. D. F., Zare R. N., and Lewis, R. S. (1998) Indigenous Polycyclic Aromatic Hydrocarbons in Circumstellar Graphite Grains from Primitive Meteorites. *Astrophys. J.* **502**, 284-295.
Messenger S., Keller L. P., Stadermann F. J., Walker R. M., and Zinner E. (2003) Samples of stars beyond the solar system: Silicate grains in interplanetary dust. *Science* **300**, 105-108.
Meyer B. S. and Zinner E. (2005) Nucleosynthesis. In *Meteorites and the Early Solar System II* (this volume).
Mostefaoui S, and Hoppe P. (2004) Discovery of Abundant In Situ Silicate and Spinel Grains from Red Giant Stars in a Primitive Meteorite. *Astrophys. J.* **613**, L149-L152.
Nagashima K., Krot A. N., and Yurimoto H. (2004) Stardust silicates from primitive meteorites. *Nature* **428**, 921-924.
Netzer N. and Elitzur M. (1993) The dynamics of stellar outflows dominated by interaction of dust and radiation. *Astrophys. J.* **410**, 701-713.
Nguyen A. N. and Zinner E. (2004) Discovery of ancient silicate stardust in a meteorite. *Science* **303**, 1496-1499.
Nittler L. R. (2003) Presolar stardust in meteorites: recent advances and scientific frontiers. *Earth & Planet. Sci. Lett.* **209**, 259-273.
Nuth III J. A. and Allen Jr. J. E. (1992) Supernovae as sources of interstellar diamonds. *Astrophysics and Space Science* **196**, 117-123.
Ozima M. and Mochizuki K. (1993) Origin of nanodiamonds in primitive chondrites: (1) Theory. *Meteoritics* **28**, 416-417.
Richter S., Ott U., and Begemann F. (1997) Tellurium-H in interstellar diamonds. *Lunar Planet. Sci.* **XXVIII**, 1185.
Roche P. F., Aitken D. K., and Smith C. H. (1993) The evolution of the 8-13 micron spectrum of supernova 1987A. *MNRAS* **261**, 522-534.
Russell S. S., Arden J. W., and Pillinger C. T. (1991) Evidence for multiple sources of diamond from primitive chondrites. *Science* **254**, 1188-1191.
Russell S. S., Arden J. W., and Pillinger C. T. (1996) A carbon and nitrogen isotope study of diamond from primitive chondrites. *Meteorit. Planet. Sci.* **31**, 343-355.
Sackmann I. J., Boothroyd A. I., and Kramer K. E. (1993) Our Sun. III. Present and future. *Astrophys. J.* **418**, 457- 468.
Sharp C. M. and Wasserburg G. J. (1995) Molecular equilibria and condensation temperatures in carbon-rich gases. *Geochim. Cosmochim. Acta* **59**, 1633-1652.

Soker N. and Harpaz A. (1999) Stellar structure and mass loss on the upper asymptotic giant branch. *MNRAS* **310**, 1158-1164.
Speck A. K., Barlow M. J., and Skinner C. J. (1997) The nature of the silicon carbide in carbon star outflows. *MNRAS* **288**, 431-456.
Speck A. K., Hofmeister A. M., and Barlow M. J. (1999) The SiC problem: Astronomical and meteoritic evidence. *Astrophys. J.* **513**, L87-L90.
Stroud R. M. and Bernatowicz T. J. (2005) Surface and internal structure of pristine presolar silicon carbide. *Lunar Planet. Sci.* **XXXVI**, Abstract #2010.
Stroud R. M., Nittler L. R., and Alexander C. M. O'D. (2004) Polymorphism in presolar Al2O3: Grains from asymptotic giant branch stars. *Science* **305**, 1455-1457.
Tielens A. G. G. M., Seab C. G., Hollenbach D. J., and McKee C. F. (1987) Shock processing of interstellar dust: Diamonds in the sky. *Astrophys. J.* **319**, L109-113.
Treffers R. and Cohen M. (1974) High-resolution spectra of cool stars in the 10- and 20- micron regions. *Astrophys. J.* **188**, 545-552.
Virag A., Zinner E., Lewis R. S., and Tang M. (1989) Isotopic compositions of H, C, and N in C diamonds from the Allende and Murray carbonaceous chondrites. *Lunar and Planetary Science* **XX**, 1158-1159.
Weigelt G., Balega Y., Blöcker T., Fleischer A. J., Osterbart R., and Winters J. M. (1998) 76 mas speckle-masking interferometry of IRC +10216 with the SAO 6 m telescope: Evidence for a clumpy shell structure. *Astron. Astrophys.* **333**, L51-L54.
Winters J. M., Le Bertre T., Jeong K. S., Helling Ch., and Sedlmayr E. (2000) A systematic investigation of the mass loss mechanism in dust forming long-period variable stars. *Astron. Astrophys.* **361**, 641-659.
Wooden D. H. (1997) Observational evidence for mixing and dust condensation in core-collapse supernovae. In *Astrophysical Implications of the Laboratory Study of Presolar Materials* (ed. T.J. Bernatowicz and E. Zinner), AIP Conf. Proc. **402**, pp. 317-376.
Wooden D. H., Rank D. M., Bregman J. D., Witteborn F. C., Tielens A. G. G. M., Cohen M., Pinto P. A., and Axelrod T. S. (1993) Airborne spectrophotometry of SN 1987A from 1.7 to 12.6 microns - Time history of the dust continuum and line emission. *Astrophys. J. Suppl.* **88,** 477-507.
Zinner E. (1998) Stellar nucleosynthesis and the isotopic composition of presolar grains from primitive meteorites. *Ann. Rev. Earth Planet. Sci.* **26**, 147-188.
Zinner E. K. (2004) Presolar grains, In *Treatise on Geochemistry*, Vol. 1, (eds. H. D. Holland, K. K. Turekian, and v. e. A. M. Davis), Elsevier, pp. 17-39.